



# Design of Gear Drives With High Gear Ratio

Faydor L. Litvin, Alfonso Fuentes, Daniele Vecchiato, and Ignacio Gonzalez-Perez  
University of Illinois at Chicago, Chicago, Illinois

## The NASA STI Program Office . . . in Profile

Since its founding, NASA has been dedicated to the advancement of aeronautics and space science. The NASA Scientific and Technical Information (STI) Program Office plays a key part in helping NASA maintain this important role.

The NASA STI Program Office is operated by Langley Research Center, the Lead Center for NASA's scientific and technical information. The NASA STI Program Office provides access to the NASA STI Database, the largest collection of aeronautical and space science STI in the world. The Program Office is also NASA's institutional mechanism for disseminating the results of its research and development activities. These results are published by NASA in the NASA STI Report Series, which includes the following report types:

- **TECHNICAL PUBLICATION.** Reports of completed research or a major significant phase of research that present the results of NASA programs and include extensive data or theoretical analysis. Includes compilations of significant scientific and technical data and information deemed to be of continuing reference value. NASA's counterpart of peer-reviewed formal professional papers but has less stringent limitations on manuscript length and extent of graphic presentations.
- **TECHNICAL MEMORANDUM.** Scientific and technical findings that are preliminary or of specialized interest, e.g., quick release reports, working papers, and bibliographies that contain minimal annotation. Does not contain extensive analysis.
- **CONTRACTOR REPORT.** Scientific and technical findings by NASA-sponsored contractors and grantees.

- **CONFERENCE PUBLICATION.** Collected papers from scientific and technical conferences, symposia, seminars, or other meetings sponsored or cosponsored by NASA.
- **SPECIAL PUBLICATION.** Scientific, technical, or historical information from NASA programs, projects, and missions, often concerned with subjects having substantial public interest.
- **TECHNICAL TRANSLATION.** English-language translations of foreign scientific and technical material pertinent to NASA's mission.

Specialized services that complement the STI Program Office's diverse offerings include creating custom thesauri, building customized databases, organizing and publishing research results . . . even providing videos.

For more information about the NASA STI Program Office, see the following:

- Access the NASA STI Program Home Page at <http://www.sti.nasa.gov>
- E-mail your question via the Internet to [help@sti.nasa.gov](mailto:help@sti.nasa.gov)
- Fax your question to the NASA Access Help Desk at 301-621-0134
- Telephone the NASA Access Help Desk at 301-621-0390
- Write to:  
NASA Access Help Desk  
NASA Center for AeroSpace Information  
7121 Standard Drive  
Hanover, MD 21076



# Design of Gear Drives With High Gear Ratio

Faydor L. Litvin, Alfonso Fuentes, Daniele Vecchiato, and Ignacio Gonzalez-Perez  
University of Illinois at Chicago, Chicago, Illinois

Prepared under Grant NAG3-2450

National Aeronautics and  
Space Administration

Glenn Research Center

Available from

NASA Center for Aerospace Information  
7121 Standard Drive  
Hanover, MD 21076

National Technical Information Service  
5285 Port Royal Road  
Springfield, VA 22100

Available electronically at <http://gltrs.grc.nasa.gov>

# **Design of Gear Drives With High Gear Ratio**

Faydor L. Litvin, Alfonso Fuentes, Daniele Vecchiato, and Ignacio Gonzalez-Perez  
University of Illinois at Chicago  
Chicago, Illinois 60607

## **Abstract**

A three part paper to describe the results of several gear drive types with a high gear ratio is presented. A single stage planetary gear train with double helical gears is described with methods to reduce transmission errors and improve load distribution by regulating backlash during assembly. A new arrangement for face gear is also described. This new mechanism can perform rotations between axes that are collinear and intersected. Finally the design and simulation of an isostatic planetary gear train is presented. Conditions that can lead to noise and vibration of the planetary gear drive are described.

# Part 1.—One-Stage Planetary Gear Train With Double-Helical Gears: Reduction of Transmission Errors and Improved Conditions of Load Distribution

## 1.1 Introduction

Planetary gear trains have been the subject of intensive research directed at determination of the dynamic response, vibration, load distribution, and other important topics (Refs. 1 to 12).

The subject of investigation performed in this part of the memorandum is one-stage planetary train with double-helical gears (Fig. 1.1).

The gear train is a multi-body system that is extremely sensitive to errors of alignment that cause large transmission errors, the possibility of edge contact, and uneven distribution of load.

The authors propose the following ideas for lessening the disadvantages mentioned above.

(1) Edge contact is avoided by localization of the bearing contact.

(2) Influence of misalignment on transmission errors is lessened due to *absorption* of discontinuous almost linear function of errors.

(3) Improved conditions of load distribution are achieved by a simple method of backlash control between the contacting surfaces. Control of backlash is accomplished in the process of assembly and becomes possible using modification of the contacting surfaces.

The contents of this part of the paper will describe: (1) preliminary design considerations and basic ideas of backlash regulation, (2) application of tooth contact analysis (TCA) for simulation of meshing and contact of all subgear drives that form a double-helical planetary gear train, (3) determination of the integrated function of transmission errors, and (4) description of an enhanced approach used for stress analysis.

## 1.2 Preliminary Design Conditions

The planetary train considered (Fig. 1.1) consists of double-helical sun and ring gears and ten planet gears of opposite directions of helices. The driving link is the sun gear, the driven one is the carrier  $c$  (not shown in the figure) on which are mounted the planet gears, while the ring gear is held at rest.

The gear ratio in transmission of motion from the sun gear  $1$  to carrier  $c$  is determined by equation

$$-\frac{\omega_1 - \omega_c}{\omega_c} = m_{13}^{(c)} = -\frac{N_3}{N_1} \quad (1.1)$$

that yields

$$\frac{\omega_c}{\omega_1} = \frac{N_1}{N_1 + N_3} \quad (1.2)$$

Designation  $m_{13}^{(c)}$  indicates the gear ratio of an inverted gear train formed by gears 1, 2, 3 where the carrier is held at rest.

The planetary gear train is designed with the observation of the following relation of tooth numbers (Refs. 8, 10, and 13)

$$\frac{N_1 + N_3}{n} = a \quad (1.3)$$

where  $a$  is an integer number,  $n$  is the number of planet gears,  $N_1$  and  $N_3$  are the tooth numbers of gears 1 and 3,  $N_2$  (tooth numbers of a planet gear) is determined as

$$N_2 = \frac{N_3 - N_1}{2} \quad (1.4)$$

The investigation has been performed for a gear train with  $N_1=41$ ,  $N_2=34$ ,  $N_3=109$ .

### 1.3 Basic Ideas

The main defects of a planetary gear train of existing design can be: (1) edge contact, (2) large transmission errors, and (3) uneven distribution of load between the gears.

These defects are caused by errors of manufacture and assembly and because the planetary train discussed is a multi-body system, since  $2n$  planet helical gears have to be in simultaneous meshing with the double-helical sun and ring gears. Here  $n$  is the number of shafts of planet gears, and remembering that two planet gears are mounted on the same shaft (Fig. 1.1).

The defects of meshing and contact mentioned above are substantially reduced by proposed modification of gear geometry and application of regulation of installment of the planet gears on the carrier of the train (see below).

**Regulation of Backlash.** A substantial improvement of conditions of load distribution is achieved by slight modification of the sun and internal gears geometry and regulation of installment of planet gears on the carrier accomplished in the process of assembly. This is achieved as follows:

(1) The screw parameters of helicoids 1,  $2_k^{(i)}$ , and 3 differ slightly each from other as the precondition for compensation of the backlash between the gears. We have chosen that  $\beta_3 < \beta_2 < \beta_1$  where  $\beta_i$  ( $i=1,2,3$ ) is the helix angle.

(2) Each planet gear  $2_k^{(i)}$  of the set of ten ( $2n=10$ ) has two degrees of freedom for its installment; ( $i=1, \dots, 5$ ;  $k=a, b$ ). Designation  $i=1, \dots, 5$  indicates that five couple of planet gears are used; designation  $k=a, b$  indicates that two planet gears  $a$  and  $b$  are installed on the same shaft.

(a) One degree-of-freedom of the planet gear is provided in assembly by turning of the planet gear about the axis of its shaft. This permits compensation of the backlash between the planet gear and ring gear or between planet gear and sun gear.

(b) The second degree-of-freedom is provided by axial displacement of the planet gear along the axis of its shaft.

Schematic illustration of regulation of backlash is represented in Figure 1.2 as follows:

(1) Figure 1.2(a) shows pitch cylinders of gears 1, 2, 3. Pitch cylinder of planet gear 2 (Fig. 1.2(a)), say left hand, is developed on plane  $\Pi$  that is coplanar to the axes of the gears. Sections of helical teeth of gears 1 and 3 are shown by straight lines (Figs. 1.2(b) and (c)). The shapes of two teeth of planet gear 2 are shown by curves since the planet gears are double crowned (see below).

(2) Gears 1 and 3 in the process of regulation are held at rest.

(3) Assume that contact of a tooth of gear 2 with the respective tooth of gear 3 is obtained by turning of planet gear 2 about its axis (Fig. 1.2(b)). However, there is a backlash  $\delta x$  between the respective teeth of gears 2 and 1.

(4) Backlash  $\delta x$  is eliminated while screw motion of gear 2 about its axis is provided (Fig. 1.2(c)). This screw motion is performed with the screw parameter of gear 3 and is equivalent to motion of two components: (a) axial displacement of teeth of gear 2, and (b) displacement in transverse direction.

Elimination of backlash  $\delta x$  is possible since the helix angles of gears 1 and 3 are slightly different.

(5) After compensation of backlash  $\delta x$ , the installment of planet gear 2 on the carrier is fixed.

(6) The regulation of backlash described above has to be performed for all ten planet gears. During the process of regulation, the backlash may be tested by application of a thin metal strip of the assigned thickness.

The regulation of backlash compensates the errors of angular installment of the planet gear on the carrier and the error of shaft angle (see section 1.4).

An idea of regulation of backlash has been applied previously for a more simple planetary train with spur gears (Ref. 13). It is extended in this study for a more complicated planetary gear train with double-helical gears.

#### **Localization of Bearing Contact and Formation of a Parabolic Shape of Transmission Errors.**

Localization of bearing contact is achieved by substitution of line contact of mating gear tooth surfaces by point contact. A predesigned parabolic function of transmission errors is applied for absorption of discontinuous almost linear functions of transmission errors caused by misalignment (Ref. 14). Application of such a function is the precondition for the reduction of transmission errors and improvement of meshing conditions wherein one pair of teeth is changed for another one (Ref. 15).

Both goals mentioned above are achieved by double-crowning of planet gears (Ref. 16) (accomplished as crowning in profile and longitudinal directions), wherein the mating gear tooth surfaces of the ring and sun gears are generated as conventional involute screw surfaces. However, the ring gear should be provided with profile crowning in order to optimize the bearing contact between the planet and ring gears.

Profile crowning of planet gears is provided by application of a skew rack-cutter of a parabolic profile in normal section (Fig. 1.3(a)). The deviation of the parabolic profile from the straight line profile is determined in the normal section as (Fig. 1.2(a))

$$\Delta x_a = a_c u_c^2 \quad (1.5)$$

where  $a_c$  is the parabola coefficient and  $u_c$  the parameter of the profile.

The geometry of the sun gear is determined considering the generation by a skew rack-cutter of a straight profile in normal section (Ref. 14).

Longitudinal crowning of a planet gear is achieved by plunging of the generating tool that might be a disk (Fig. 1.3(b)), or a grinding worm (Fig. 1.3(c)). Tool plunging is achieved by variation of shortest center distance accomplished by a parabolic function (Ref. 17). The plunge equation is represented as

$$E = E^{(0)} - a_{pl} l^2 \quad (1.6)$$

Here,  $a_{pl}$  is the parabola coefficient,  $l$  is the parameter of motion of the tool,  $E^{(0)}$  is the initial center distance between the pinion and the tool, and  $E$  is the current center distance.

## 1.4 Application of TCA for determination of Transmission Errors and Bearing Contact

Tooth Contact Analysis (TCA) is designated for simulation of meshing and contact of gear tooth surfaces of a misaligned gear drive. TCA in this paper is applied for the following purposes: (1) as proof of the effectiveness of regulation of backlash, (2) for determination of the path of contact and transmission errors of misaligned gear drives. The contents of this section cover algorithms of TCA: (1) for a conventional gear drive with two gears, and (2) for a double helical subtrain gear drive, wherein the carrier is held at rest and the rotation is performed from the sun gear to the ring gear.

**Conventional Gear Drive.** The gear drive consists of two gears  $I$  and  $2$ . The tangency of surfaces is considered in a fixed coordinate system  $S_f$ . The TCA algorithm represents the conditions of continuous tangency of contacting surfaces  $\Sigma_1$  and  $\Sigma_2$  by the following vector equations

$$\mathbf{r}_f^{(1)}(u_1, \theta_1, \phi_1) = \mathbf{r}_f^{(2)}(u_2, \theta_2, \phi_2) \quad (1.7)$$

$$\mathbf{n}_f^{(1)}(u_1, \theta_1, \phi_1) = \mathbf{n}_f^{(2)}(u_2, \theta_2, \phi_2) \quad (1.8)$$

Here:  $(u_i, \theta_i)$  are the surface parameters;  $\phi_i$  is the angle of rotation of gear  $i$  ( $i = 1, 2$ );  $\mathbf{r}_f^{(i)}(u_i, \theta_i, \phi_i)$  is the position vector of surface  $\Sigma_i$  in fixed coordinate system  $S_f$ ;  $\mathbf{n}_f^{(i)}(u_i, \theta_i, \phi_i)$  is the unit normal to surface  $\Sigma_i$  in fixed coordinate system  $S_f$ .

Vector Equations (1.7) and (1.8) yield five independent scalar equations represented as

$$f_i(u_1, \theta_1, \phi_1, u_2, \theta_2, \phi_2) = 0 \quad (i = 1, \dots, 5) \quad (1.9)$$

Note that vector Equation (1.8) provides only two independent scalar equations since  $|\mathbf{n}_f^{(1)}| = |\mathbf{n}_f^{(2)}| = 1$ .

The application of equation system (1.9) for TCA is an iterative process (Ref. 14) that is performed as follows:

- (1) It is assumed that there is a set of parameters

$$P^{(0)}(u_1^{(0)}, \theta_1^{(0)}, \phi_1^{(0)}, u_2^{(0)}, \theta_2^{(0)}, \phi_2^{(0)}) \quad (1.10)$$

that satisfies equation system (1.9).

- (2) One of the unknowns, say  $\phi_1$ , is chosen as an input parameter and the following inequality at  $P^{(0)}$  is observed

$$\Delta_1 = \begin{vmatrix} \frac{\partial f_1}{\partial u_1} & \frac{\partial f_1}{\partial \theta_1} & \frac{\partial f_1}{\partial u_2} & \frac{\partial f_1}{\partial \theta_2} & \frac{\partial f_1}{\partial \phi_2} \\ \dots & \dots & \dots & \dots & \dots \\ \frac{\partial f_5}{\partial u_1} & \frac{\partial f_5}{\partial \theta_1} & \frac{\partial f_5}{\partial u_2} & \frac{\partial f_5}{\partial \theta_2} & \frac{\partial f_5}{\partial \phi_2} \end{vmatrix} = 0 \quad (1.11)$$

(3) Then, in accordance to the Theorem of Implicit Function System Existence (Ref. 18), equation system (1.9) can be solved in the neighborhood of  $P^{(0)}$  by functions

$$\phi_2(\phi_1), u_1(\phi_1), \theta_1(\phi_1), u_2(\phi_1), \theta_2(\phi_1) \quad (1.12)$$

(4) Applying the iterative process mentioned above it becomes possible to determine functions (1.12) for different values of  $\phi_1$  and complete the whole cycle of meshing.

(5) Using transmission function  $\phi_2(\phi_1)$ , it becomes possible to determine the function of transmission errors as

$$\Delta\phi_2(\phi_1) = \phi_2(\phi_1) - \frac{N_1}{N_2}\phi_1 \quad (1.13)$$

(6) Path of contact of surface  $\Sigma_i$  ( $i=1,2$ ) is determined as

$$\mathbf{r}_i(u_i(\phi_1), \theta_i(\phi_1)) \quad (1.14)$$

where  $\mathbf{r}_i(u_i(\phi_1), \theta_i(\phi_1))$  is the vector function that represents  $\Sigma_i$  in coordinate system  $S_i$ .

**Application of TCA to a Subgear Drive.** Subgear drives are formed by a certain number of the gears that are applied in the double-helical planetary gear train.

We differentiate a single subgear drive and a twin subgear drive as follows. The single subgear drive is formed by a helical ring gear  $3_a$ , helical planet gear  $2_a$ , and helical sun gear  $1_a$ . The twin subgear drive is formed by a double-helical internal ring gear  $3$  ( $3_a$  and  $3_b$ ), two helical planet gears  $2_a$  and  $2_b$  with opposite directions of helices, and a double-helical external sun gear  $1$  ( $1_a$  and  $1_b$ ). Once the assembly of the two helical planet gears is accomplished, the pair of planet gears constitute a rigid body. The rotations performed for a single and twin subgear drives, respectively, are considered as provided from the sun gear via planet gear (gears) to the ring gear while the carrier is held at rest.

The concepts of single and twin subgear drives are applied wherein TCA and stress analysis are considered.

The TCA of a twin subgear drive requires the following steps:

**Step 1.** Tooth surfaces of gears  $1_k, 2_k^{(i)}$  and  $3_k$ , ( $i=1, k=a,b$ ) are represented in fixed coordinate system  $S_f$ . The single subgear drive formed by gears  $1_k, 2_k^{(1)}$  and  $3_k$  ( $k=a$ ) is considered. Rotation of gears are represented by three parameters  $\phi_1, \phi_{2a}^{(1)}, \phi_{3a}^{(1)}$ .

**Step 2.** Conditions of tangency of gears  $1_a$  and  $2_a^{(1)}$ , and gears  $2_a^{(1)}$  and  $3_a$  provide ten independent equations that are similar to Equation (9). These equations contain eight surface parameters and three motion parameters  $\phi_1, \phi_{2a}^{(1)}, \phi_{3a}^{(1)}$ . Considering  $\phi_1$  as the input parameter, we may obtain from the TCA computer program the transmission function  $\phi_{3a}^{(1)}(\phi_1)$  in case of aligned and misaligned single subgear drive.

The solution of ten non-linear equations can be simplified by representing them as two sub-systems of five equations each, in which the solution as function  $\phi_{2a}^{(1)}(\phi_1)$  obtained by the first sub-system will be the input parameter for the second sub-system.

**Step 3.** The approach discussed in Steps 1 and 2 has to be applied for the single subgear drive with planet gear  $k=b$ . At the performed simulation, functions of transmission errors  $\Delta\phi_{3a}^{(1)}(\phi_1)$  and  $\Delta\phi_{3b}^{(1)}(\phi_1)$  of both single subgear drives are obtained independently based on the assumption that meshing exist at four points simultaneously.

**Step 4.** The transmission function of the twin subgear drive is determined as

$$\Delta\phi_3^{(1)}(\phi_1) = \max\{\Delta\phi_{3a}^{(1)}(\phi_1), \Delta\phi_{3b}^{(1)}(\phi_1)\} \quad (1.15)$$

The procedure discussed above may be applied for determination of transmission errors for all twin subgear drives of the planetary gear drive. Figure 1.4(a) shows functions of transmission errors  $\Delta\phi_3(\phi_1)$  obtained for five twin subgear drives. It is obvious that due to the existence of transmission errors, only one planet gear may be in meshing with gears 3 and 1 (if elastic deformations are not taken into account). The transmission errors are caused by double-crowning and angular errors of installment of planet gears on the carrier (see numerical example 1 below).

Points  $M_i$  ( $i = 1, 5$ ) in Figure 1.4(a) correspond to the transmission errors  $\Delta\phi_3^{(i)}(\phi_1^*)$  where  $\phi_1^*$  is the instantaneous angle of rotation of the sun gear 1. It is easy to be verified from the graph that only planet gear 2<sup>(2)</sup> is in mesh. The magnitude  $|M_2M_i|$  ( $i = 1, 3, 4, 5$ ) indicate the backlash between the teeth of gears 2<sup>(2)</sup> and 2<sup>(i)</sup>.

The paths of contact in a twin subgear drive are shown in Figure 1.4(c).

## 1.5 Integrated Function of Transmission Errors

The integrated function of transmission errors is obtained with the assumption that the backlash between the planet gears and the mating gears 1 and 3 is minimized by regulation of the axial position of the planet gears. However, since the backlash is not constant even after regulation, only one of the planet gear may be still in mesh. Small elastic deformation enables all planet gears will be in mesh.

Figure 1.4(b) shows that after regulation the maximal magnitude of transmission errors is substantially reduced. This statement is based on comparison of Figures 1.4(a) and (b).

**Numerical Example 1.1.** The design parameters of the planetary gear drive are given in Table 1.1. Errors of installment of planet gears on the carrier are designated in Table 1.2 as  $\Delta E_x$ , where  $\Delta E_x$  is the error of position of the planet gear on the carrier measured in the direction that is perpendicular to the shortest center distance. Designation  $\Delta Z^{(i)}$  ( $i=1, 2$ ) indicate the axial displacement of the planet gear that is applied for elimination of the backlash. Designations  $\Delta Z^{(1)}$  and  $\Delta Z^{(2)}$  indicate the approximate and precise displacements. Here  $\Delta Z^{(1)}$  is obtained from the equation

$$\Delta E_x = \frac{\Delta Z^{(1)} \sin(\beta_1 - \beta_3)}{2 \cos \beta_1 \cos \beta_3} \quad (1.16)$$

while  $\Delta Z^{(2)}$  is obtained from the results of TCA in order to balance function of transmission errors  $\Delta\phi_3^{(i)}(\phi_1)$  ( $i = 1, 5$ ).

The helix angles have been chosen as

$$\beta_1=10.25^\circ, \beta_2=10.00^\circ, \beta_3=9.75^\circ$$

Figure 1.4(a) shows that only planet gear 2<sup>(2)</sup> can be in mesh in the misaligned planetary gear train. The backlash  $|M_2M_i|$  ( $i = 1, 3, 4, 5$ ) is of a large magnitude and therefore planet gears that differ from 2<sup>(2)</sup> may be in mesh after substantial elastic deformations.

Figure 1.4(b) shows that the difference of functions  $\Delta\phi_3^{(i)}(\phi_1)$  is reduced after axial placement regulation (application of  $\Delta Z^{(2)}$ , see Table 1.2). Therefore, lessened elastic deformations are required for more uniform distribution of load between the planet gears.

**Numerical Example 1.2.** The proposed approach may be applied as well for elimination of the backlash caused by misalignment  $\Delta\gamma$ , as the change of the shaft angle.

Figure 1.5(a) shows functions of transmission errors  $\Delta\phi_{3a}^{(l)}(\phi_l)$  and  $\Delta\phi_{3b}^{(l)}(\phi_l)$  obtained for  $\Delta\gamma=3$  arcmin. Designations  $\Delta\phi_{3a}^{(l)}(\phi_l)$  and  $\Delta\phi_{3b}^{(l)}(\phi_l)$  indicate transmission errors of gear 3 when 3 will be in mesh with planet gears  $2_a^{(l)}$  and  $2_b^{(l)}$ . Since functions  $\Delta\phi_{3a}^{(l)}(\phi_l)$  and  $\Delta\phi_{3b}^{(l)}(\phi_l)$  differ each from other, simultaneous contact of gears  $2_a$  and  $2_b$  cannot be achieved. However, we may compensate this defect substantially, by regulation of installment of planet gears  $2_a^{(l)}$  and  $2_b^{(l)}$ .

Figure 1.5(b) shows functions  $\Delta\phi_{3a}^{(l)}(\phi_l)$  and  $\Delta\phi_{3b}^{(l)}(\phi_l)$  after regulations of installment of gears  $2_a^{(l)}$  and  $2_b^{(l)}$  on the carrier. The reduction of difference  $|\Delta\phi_{3a}^{(l)}(\phi_l)-\Delta\phi_{3b}^{(l)}(\phi_l)|$  is in favor of more uniform distribution of load in the planetary train. The regulation of axial installment of planet gears  $2_a^{(l)}$  and  $2_b^{(l)}$  has to be performed for all ten planet gears.

## 1.6 Stress Analysis

Stress analysis has been performed for twin subgear drives of the new and previous designs by considering the following conditions:

(1) The twin subgear drive is formed by: (a) a double-helical ring gear and sun gear, and (b) a couple of helical planet gears are mounted on the same shaft.

(2) The carrier is held at rest, the sun gear is the driving one, and the resisting torque is applied to the ring gear.

(3) Conventional involute helical gear tooth surfaces are applied in the existing design. Such surfaces are in line contact, but point contact occurs since a misaligned subgear drive with the error of the shaft angle  $\Delta\gamma=3$  arcmin has been considered.

(4) Gear tooth surfaces of the new design are already in point contact due to the localization of bearing contact.

The stress analysis performed is based on finite element method (Ref. 19) and application of a general computer program (Ref. 20).

**Development of Finite Element Models.** The approach developed for automatic generation of finite element models and application of stress analysis by a general purpose computer program (Ref. 20) is accomplished as follows (Ref. 17):

**Step 1.** Tooth surface equations of sun, planet and ring gears and portions of corresponding rim are considered for determination of the volumes of the designed bodies. Figure 1.6(a) shows the designed body of one-tooth model.

**Step 2.** The designed volume of each tooth of the model is divided into six subvolumes using auxiliary intermediate surfaces 1 to 6 as shown in Fig. 1.6(b).

**Step 3.** Node coordinates are determined analytically considering the number of desired elements in longitudinal and profile directions (Fig. 1.6(c)).

**Step 4.** Generation of the model by finite elements (using the nodes determined in previous step) is accomplished as shown in Fig. 1.6(d).

**Step 5.** Setting of boundary conditions is accomplished automatically and is shown in Fig. 1.7 for the case of a three-tooth model.

The following ideas are applied:

(1) Nodes on the two sides and the bottom part of the portion of the rim for each member of the sun-gear are considered as fixed. Two members are considered since we have double-helical gears.

(2) Nodes on the two sides and the bottom part of the portion of the rim for each member of the planet gear form the rigid surface 2. Considering that the planet gear is in mesh with the sun and ring gears, four members are taken into account for determination of rigid surface 2.

(3) A reference node  $N_2$  located on the axis of the planet gear is used as the reference point of the previously defined rigid surface 2. Reference point  $N_2$  and the rigid surface 2 constitute the rigid body 2.

(4) Only one degree-of-freedom is defined as free at the reference point  $N_2$  (it is rotation about the planet gear axis), while all other degrees of freedom are fixed. This will allow free rotation of the planet gear.

(5) Nodes on the two sides and the bottom part of the portion of the rim for each member of the ring gear form the rigid surface 3.

(6) A reference node  $N_3$  located on the axis of the ring gear is used as the reference point of the rigid surface 3. Reference point  $N_3$  and the rigid surface 3 constitute the rigid body 3.

(7) Only one degree of freedom is defined as free at the reference point  $N_3$  (rotation about the ring gear axis) while all other degrees of freedom are fixed. Application of a torque  $T$  in rotational motion at the reference point  $N_3$  allows to apply such torque to the ring gear model. The planet gear will transmit such torque to the sun gear model that is held at rest.

**Step 6.** The contact algorithm of the finite element analysis computer program (Ref. 20) requires definition of contacting surfaces. This approach makes it possible to identify automatically all the elements of the model required for the formation of such surfaces.

The principal characteristics of the described approach are as follows:

(1) Finite element models of the gear drive can be automatically obtained for any position of pinion and gear obtained from TCA. Stress convergence is assured because there is at least one point of contact between the contacting surfaces.

(2) Assumption of load distribution in the contact area is not required since the algorithm of contact from the general computer program (Ref. 20) is used to obtain the contact area and stresses.

(3) Finite element models of any number of teeth can be obtained. Figure 1.8 shows the finite element model of three pairs of contacting teeth.

Considering that the models are constituted by several teeth, the following advantages are obtained:

(1) Boundary conditions are far enough from the loaded areas of the teeth.

(2) Simultaneous meshing of two pairs of teeth can occur due to the elasticity of surfaces. Therefore, the load transition at the beginning and at the end of the path of contact can be studied.

**Numerical Example 1.3.** The finite element analysis has been performed for the following cases mentioned above:

(1) Planetary gear trains with modified double-helical gears are applied.

(2) Conventional involute double-helical gears are applied in the planetary gear train.

In case (1), planet gears are double-crowned (in longitudinal and profile directions), the ring gear is profile crowned, and the sun gear is a conventional one. Helix angles of sun and ring gears slightly differ each from other for the purpose of regulation (see Example 1).

The finite element analysis has been performed by using the design parameters shown in Table 1 and the following conditions:

(1) The error of misalignment has been considered as the change of the shaft angle  $\Delta\gamma=3$  arcmin.

(2) The contact stresses have been determined in both cases at one angular position of gears 1, 2, and 3.

(3) In the case of a new design, regulation of backlash has been performed as described in Numerical Example 2: independent axial displacements of planet gears  $2_a$  and  $2_b$  have allowed to obtain distribution of load between the two gears, even in case of error  $\Delta\gamma$ .

Four contacting models, similar to those shown in Figure 1.7, based on application of a three teeth finite element model, have been designed (Fig. 1.8). Two of these models correspond to the contact of two planet gears and the sun gear and the other two models correspond to the contact of the two planet gears and the ring gear. The maximum of the function of transmission errors  $\Delta\phi_3(\phi_1)$  is obtained at the chosen point of contact. 8 node brick elements (Ref. 20) of first order (enhanced by incompatible modes to improve their bending behavior) have been used to form the finite element mesh. The total number of elements is 147,632 with 175,563 nodes. The material is steel with the properties of Young's Modulus  $E=2.068 \cdot 10^5$  MPa and Poisson's ratio 0.29. A torque of 500 Nm has been applied to the ring gear.

The highest contact stresses are obtained on tooth surfaces of the planet gear being in mesh with the sun gear. Figures I.9(a) and I.9(b) illustrate the teeth of two planet gears in meshing with a double-helical sun gear for cases (1) and (2), respectively. An error of 3 arcmin of the shaft angle is considered in both cases. Figure 1.9(a) shows that the load is shared by the two planet gears after regulation is applied. Figure 1.9(b) shows that only one planet gear is under the load and edge contact occurs.

The performed stress analyses for the cases mentioned above and the results of TCA (see section 1.4) confirm the advantages of the proposed modification of geometry.

## 1.7 Conclusions

Based on the performed research, the following conclusions may be drawn:

(1) The bearing contact is localized due to the mismatch of generating tools applied for generation of planet gears and ring and sun gears.

(2) Double-crowning of planet gears is provided by the mismatch of generating tools and tool plunging accomplished by variation of shortest center distance between the tool and the generated planet gear. The variation of shortest center distance is controlled by a parabolic function.

(3) Manufacture of planet gears of modified geometry may be accomplished by application of a grinding disk or a grinding worm.

(4) Almost uniform distribution of load between the planet gears is achieved by regulation of backlash in the process of assembly accomplished as follows:

(a) Two degree-of-freedom are foreseen for the installment of each planet gear on the carrier accomplished by: (1) turning about its axis, and (2) screw motion about the axis of planet gear with the screw parameter of the mating gear.

(b) Two slightly different screw parameters are provided for the helicoids that represent the tooth surfaces of the ring gear and the sun gear.

(5) Simulation of meshing and contact of a misaligned planetary gear train is performed by application of the developed computer program. The results of simulation have confirmed substantial reduction of transmission errors as the result of proposed regulation of installment of planet gears on the carrier.

(6) Stress analysis has been performed for the new and existing designs. The advantage of the new design is the result of a more uniform load distribution.

## References

1. Chatterjee, G., and Tsai, L.W., *Computer-Aided Sketching of Epicyclic-Type Automatic Transmission Gear Trains*, Journal of Mechanical Design, Vol. 118, pp. 405–411.
2. Chen, J.L, and Tseng, C.H., *Design Considerations for Assemble in Planetary Gear Trains*, Proceedings of the International Conference on Gearing, Transmissions, and Mechanical Systems, Nottingham Trent University UK, pp. 157–166, 2000.

3. Hori, K., and Hayashi, I., *Optimization of the Profile-Shift Coefficients of Conventional Mechanical Paradox Planetary Gear Drives to Obtain the Maximum Efficiency*, Power Transmission and Gearing Conference, ASME DE-Vol. 88, 1996.
4. Hori, K., and Hayashi, I., *Improvement of Efficiency of 3K-Type Mechanical Paradox Planetary Gear Drive by Equalizing Approach and Recess-Contact Ratios*, Power Transmission and Gearing Conference, ASME DE-Vol. 88, 1996.
5. Ishida, T., and Hidaka, T., *Effects of Assemble and Manufacturing Errors on Transmission Error of Planetary Gears*, Proceedings of the International Power Transmission and Gearing Conference, DE-Vol. 43-1, pp. 375-381, 1992.
6. Kahraman, A., *Load Sharing Characteristics of Planetary Transmissions*, Mechanism and Machine Theory, Vol. 129, pp. 1151-1165, 1994.
7. Kahraman, A., and Vijajakar, S., *Effect of Internal Gear Flexibility on the Quasi-Static Behaviour of a Planetary Gear Set*, Journal of Mechanical Design, Vol. 123, pp. 408-415, 2001.
8. Kudrjatzjev, V.N. et al., *Computation and Design of Gear Reducers*, Politehnika, S. Peterburg, 1993.
9. Lin, J., and Parker, R.G., *Analytical Characterization of the Unique Proprieties of Planetary Gear Free Vibration*, Journal of Vibration and Acoustics, Vol. 121, pp. 316-321, 1999.
10. Lynwander, P., *Gear Drive System-Design and Application*, Marcel Dekker Inc., 1983.
11. Saada, A., and Velez, P., *An Extended Model for the Analysis of the Dynamic Behaviour of Planetary Trains*, Journal of Mechanical Design, Vol. 117, pp. 241-247, 1995.
12. Velez, P., and Flamand, L., *Dynamic Response of Planetary Trains to Mech Parametric Excitations*, Journal of Mechanical Design, Vol. 118, pp. 7-14, 1996.
13. Litvin, F.L., Vecchiato, D., Demenego, A. et al., *Design of One Stage Planetary Gear Train with Improved Conditions of Load Distribution and Reduced Transmission Errors*, Journal of Mechanical Design, Vol. 124, 2002.
14. Litvin, F.L., and Fuentes, A., *Gear Geometry and Applied Theory, Second Edition*, Cambridge University Press, New York, 2004.
15. Litvin, F.L., Wang, A.G., and Handschuh, R.F., *Computerized Generation and Simulation of Meshing and Contact of Spiral Bevel Gears with Improved Geometry*, Computer Methods in Applied Mechanics and Engineering, Vol. 158, pp. 35-64, 1998.
16. Litvin, F.L. et al., *Helical and spur gear drive with double crowned pinion tooth surfaces and conjugated gear tooth surfaces*, US Patent Office, Patent No. 6,205,879, 2001.
17. Litvin, F.L., Fuentes, A., Gonzalez-Perez, I., Carnevali, L., and Sep, T.M., *New Version of Novikov-Wildhaber Helical Gears: Computerized Design, Simulation of Meshing and Stress Analysis*, Computer Methods in Applied Mechanics and Engineering, Vol. 191, pp. 5707-5740, 2002.
18. Korn, G.A. and Korn, T.M., *Mathematics Handbook for Scientist and Engineers*, McGraw-Hill, Inc., 2nd Ed., 1968.
19. Zienkiewicz, O.C. and Taylor, R.L., *The Finite Element Method*, John Wiley & Sons, 5th Ed., 2000.
20. Hibbit, Karlsson & Sirensen, Inc., *ABAQUS/Standard User's Manual*, 1800 Main Street, Pawtucket, RI 02860-4847, 2000.

TABLE 1.1.—DESIGN PARAMETERS

|  |                        |
|--|------------------------|
| Number of teeth of the sun gear, $N_1$   | 41                     |
| Number of teeth of the planet gear, $N_2$  | 34                     |
| Number of teeth of the ring gear, $N_3$  | 109                    |
| Module, $m$  | 2.0 mm                 |
| Normal pressure angle, $\alpha_n$  | 20°                    |
| Helix angle, $\beta$   | 10°                    |
| Face width of each member, $B$   | 30 mm                  |
| Distance between the members, $F$  | 10 mm                  |
| Primitive radius of grinding disk, $r_D$   | 100 mm                 |
| Parabolic coefficient on driving profile of planet gear rack cutter, <sup>a</sup> $a_{cd}$ | 0.008 mm <sup>-1</sup> |
| Parabolic coefficient on coast profile of planet gear rack cutter, <sup>a</sup> $a_{cc}$   | 0.005 mm <sup>-1</sup> |
| Parabolic coefficient of plunging for planet gears, <sup>a</sup> $a_{pl}$                  | 0.002 mm <sup>-1</sup> |
| Parabolic coefficient of ring gear rack cutter, <sup>a</sup> $a_{cr}$                      | 0.002 mm <sup>-1</sup> |
| Helix angle of sun gear, <sup>a</sup> $\beta_1$  | 10.25°                 |
| Helix angle of ring gear, <sup>a</sup> $\beta_3$   | 9.75°                  |

<sup>a</sup>Data applied to a planetary gear train with double crowned involute gears.

TABLE 1.2.—AXIAL DISPLACEMENTS  $\Delta Z$ 

| Planetary gear | $\Delta E_x$ ,<br>μm | $\Delta Z^{(1)}$ ,<br>mm<br>(from Eq. (16)) | $\Delta Z^{(2)}$ ,<br>mm<br>(from TCA) |
|----------------|----------------------|---|--|
| $2^{(1)}$      | 0                    | 0   | 0                                      |
| $2^{(2)}$      | 20                   | -4.44                                       | -4.6                                   |
| $2^{(3)}$      | -20                  | 4.44  | 4.6                                    |
| $2^{(4)}$      | 5                    | -1.11                                       | -1.15                                  |
| $2^{(5)}$      | -5                   | 1.11  | 1.15                                   |

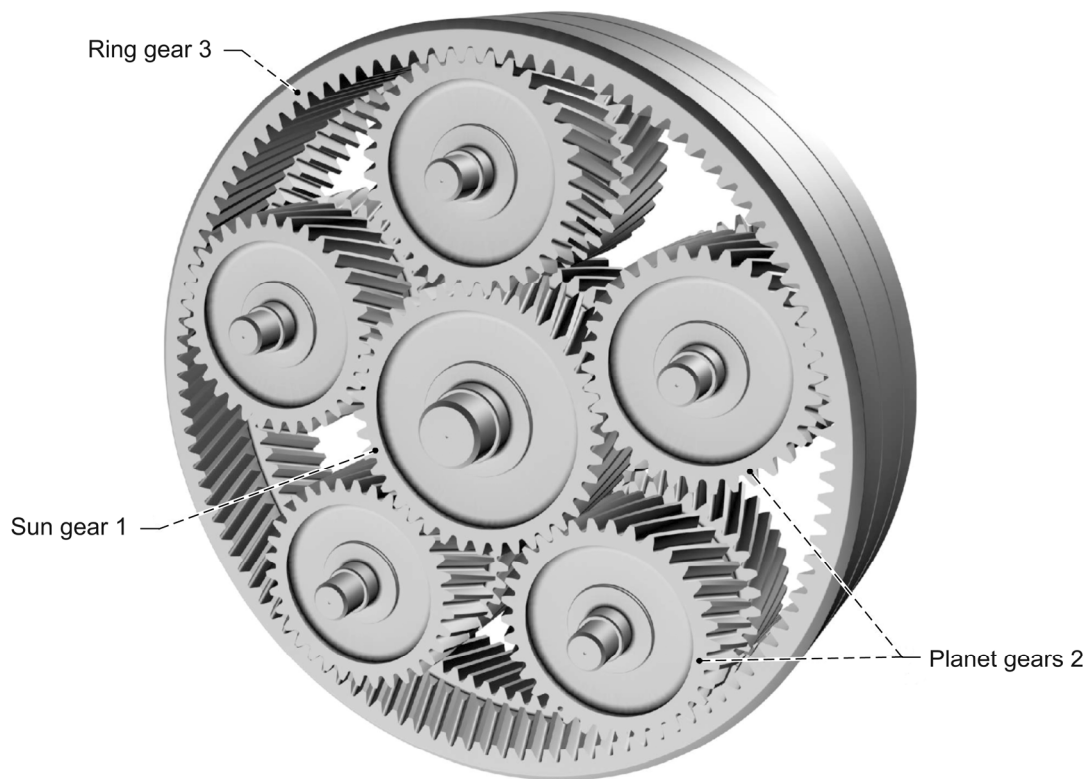


Figure 1.1.—Schematic of planetary gear train.

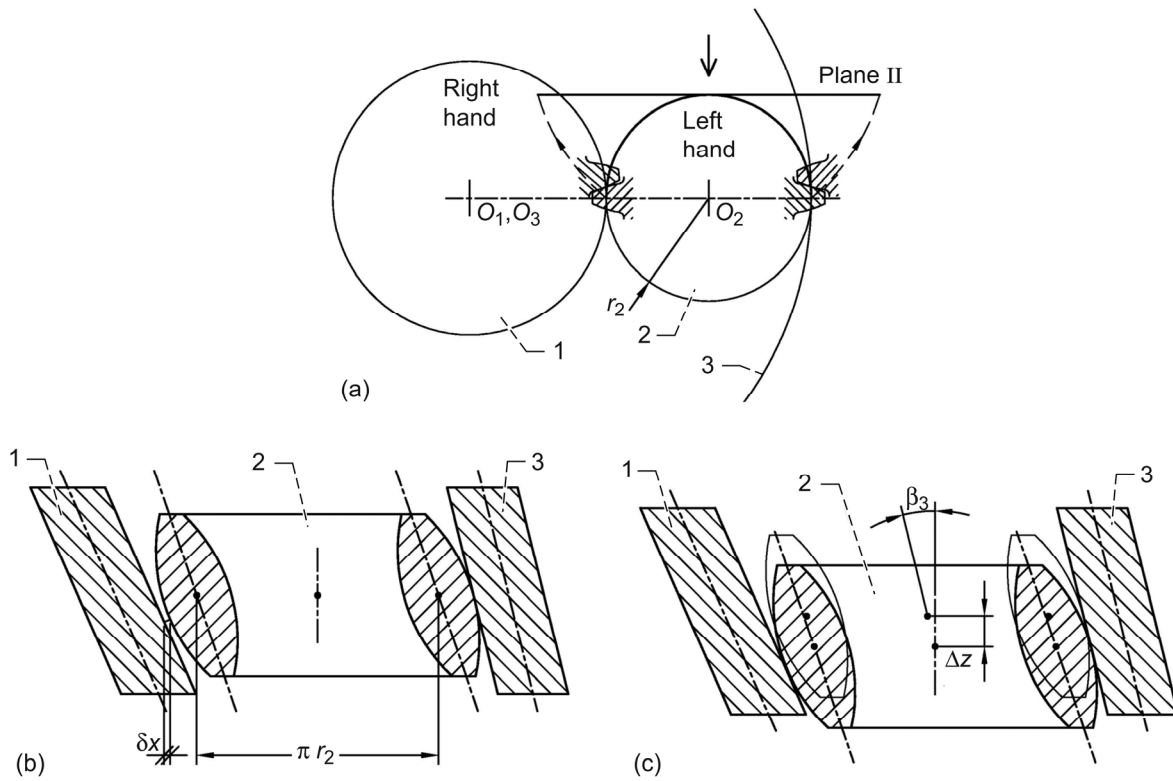


Figure 1.2.—Illustration of regulation of backlash. (a) Representation of pitch cylinders of gears 1, 2, 3 and plane II. (b) Illustration of tangency of gears 2 and 3 and existence of backlash  $\delta x$ . (c) Elimination of backlash  $\delta x$ .

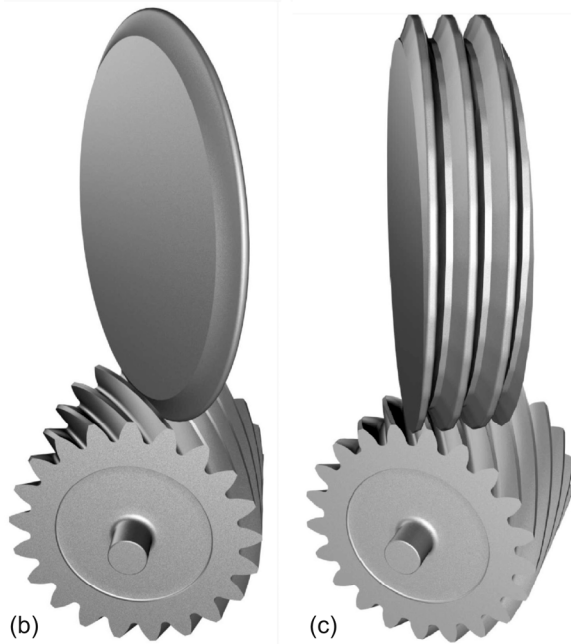
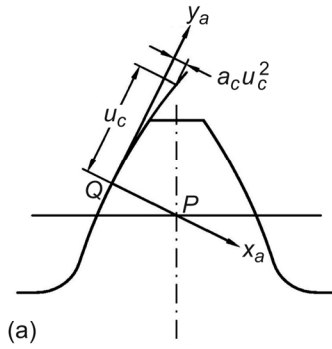


Figure 1.3.—Generating tools. (a) Parabolic profile of rack-cutter. (b) Generating disk. (c) Generating worm.

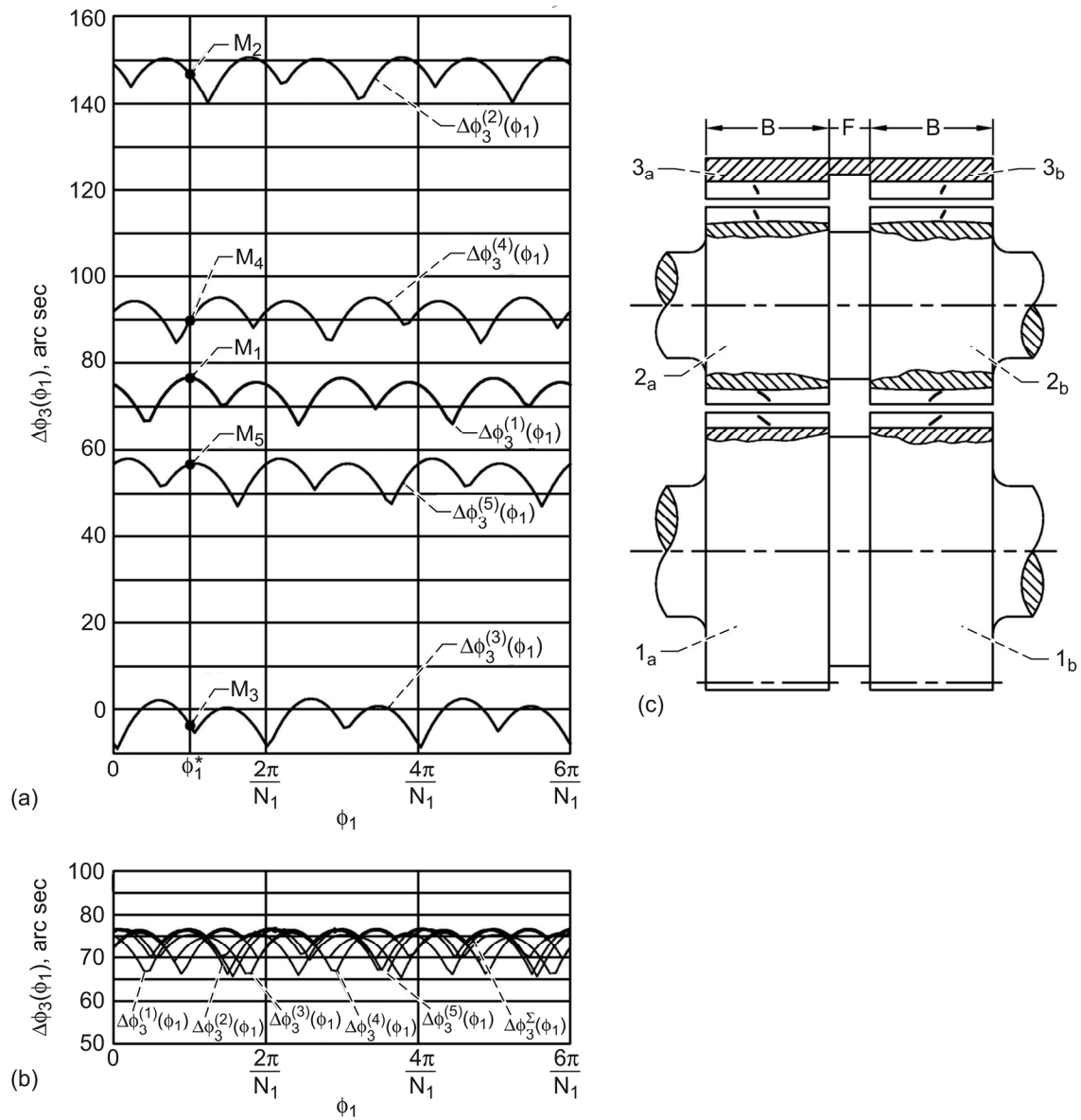


Figure 1.4.—Function of transmission errors  $\Delta\phi_3^{(1)}(\phi_1)$  caused by double crowning and errors  $\Delta E_x$  of planetary gears.

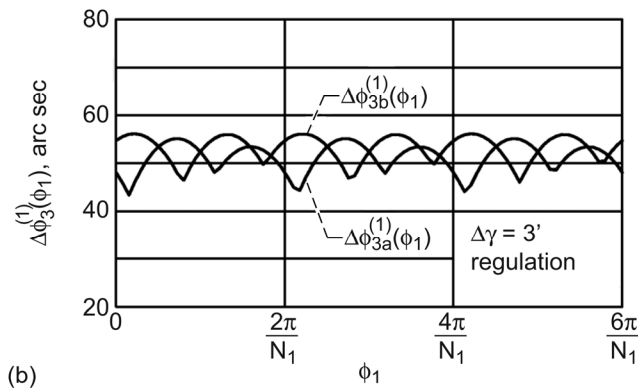
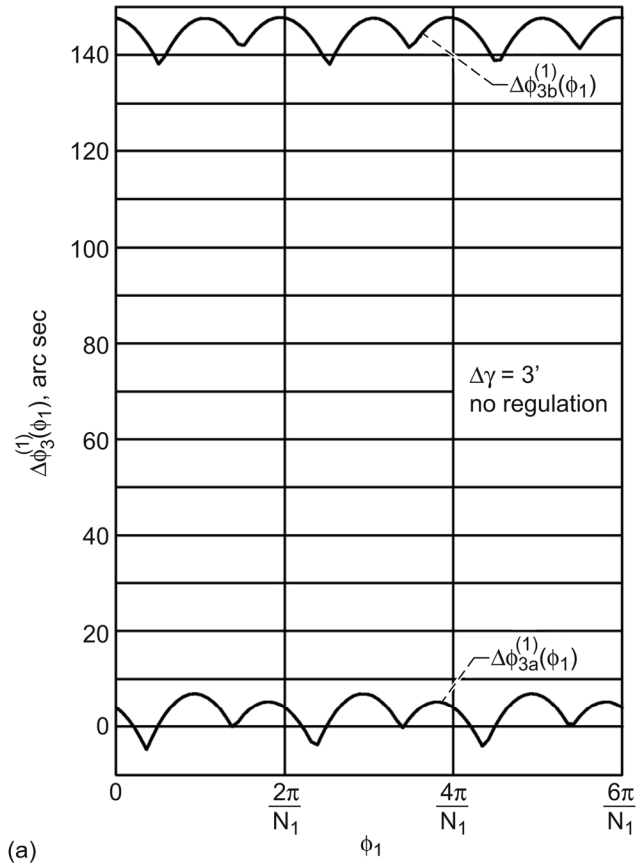


Figure 1.5.—Functions of transmission errors  $\Delta\phi_{3k}^{(1)}(\phi_1)$  ( $k = a, b$ ) caused by double crowning and error  $\Delta\gamma$  of planetary gear 2<sup>(1)</sup>.  
 (a) Transmission errors before regulation. (b) Transmission errors after regulation.

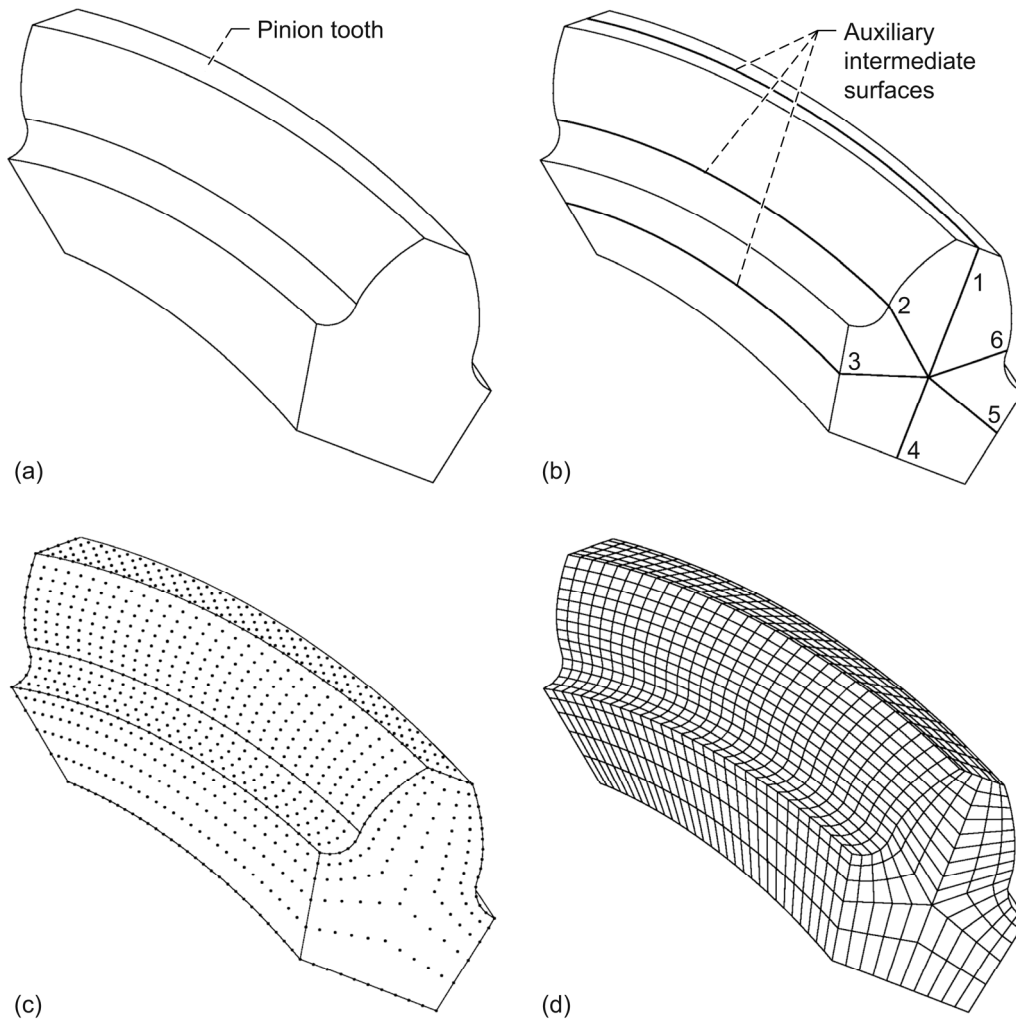


Figure 1.6.—Illustrations. (a) Volume of designed body. (b) Auxiliary intermediate surfaces. (c) Determination of nodes for the whole volume. (d) Discretization of the volume by finite elements.

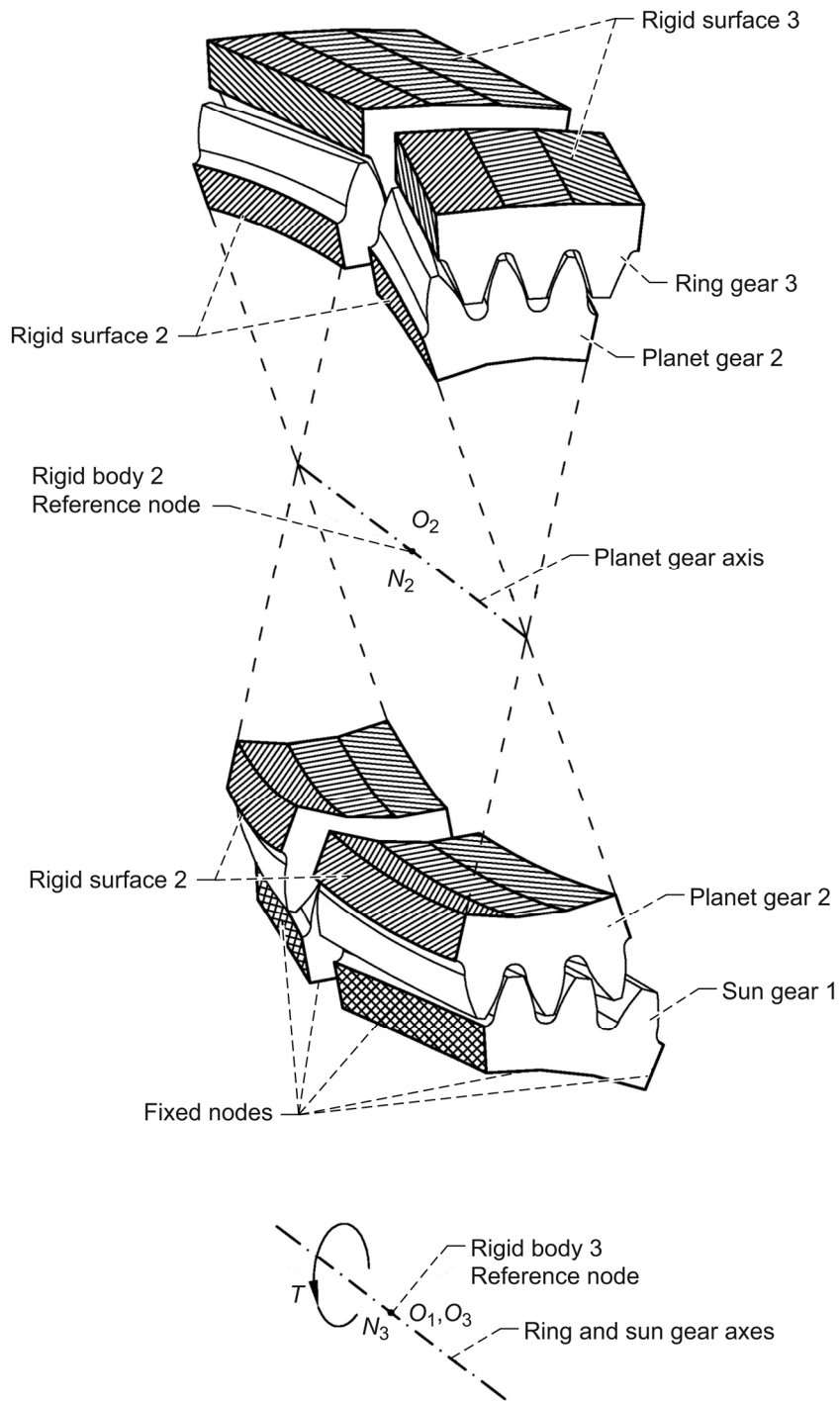


Figure 1.7.—Schematic illustration of boundary conditions for the sun, ring, and planet gears.

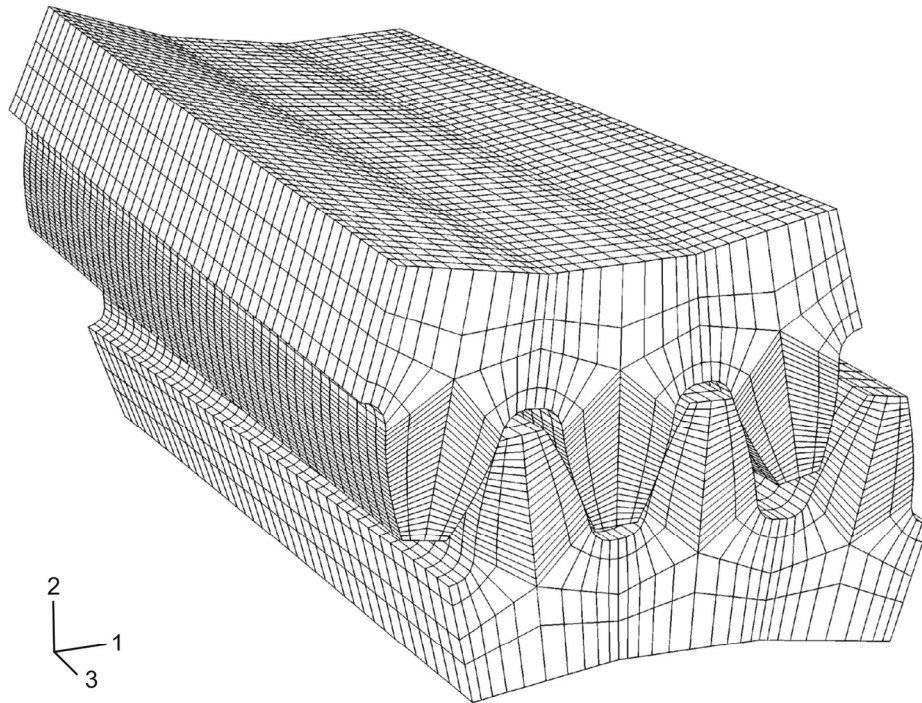
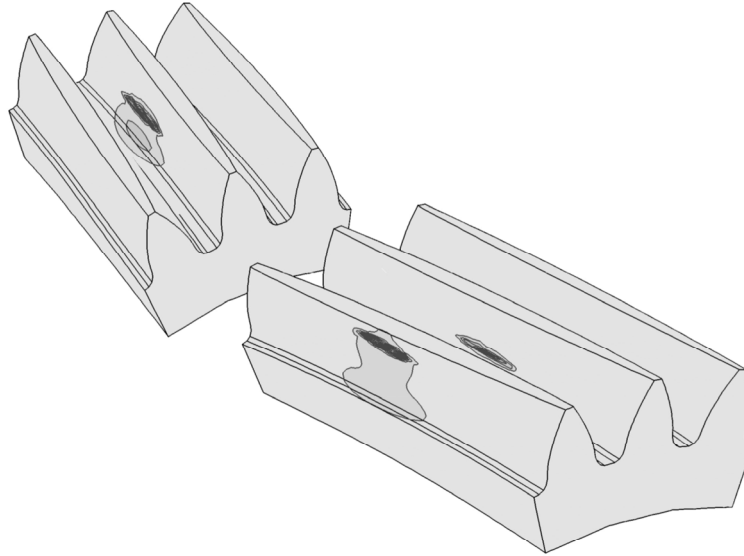
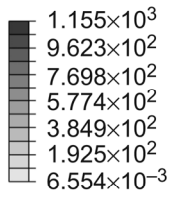


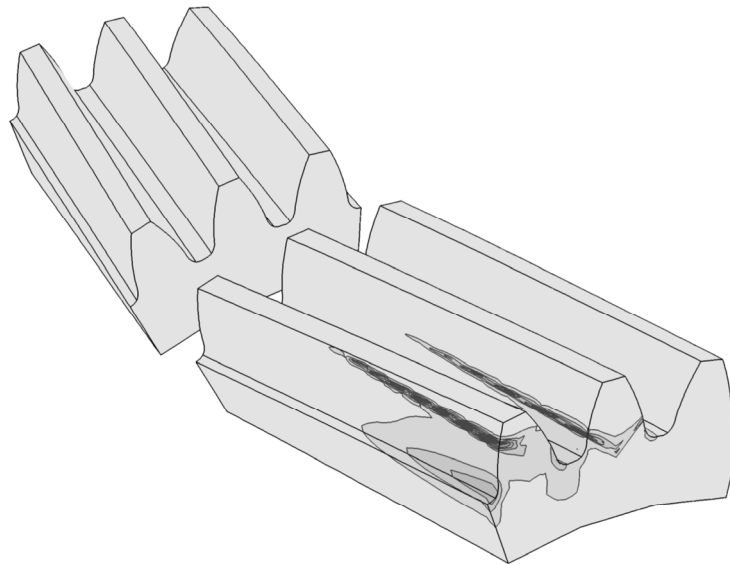
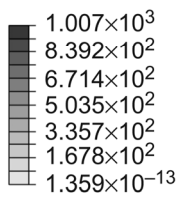
Figure 1.8.—Three tooth finite element model.

Von Mises stress,  
MPa



(a)

Von Mises stress,  
MPa



(b)

Figure 1.9.—Contact stresses of two planet gears being in mesh with a double helical sun gear. (a) In case of modified geometry. (b) Conventional geometry.



## Part 2.—Design of Planetary Gear Drives With Face Gears

### 2.1 Introduction

The planetary gear train proposed (Fig. 2.1) is a new development that may be applied as a reducer, a multiplier, or a differential. The train is formed by: (1) co-axial face-gears 1 and 4, and (2) carrier  $c$  at which are mounted helical pinions 2 and 3. Pinions 2 and 3 are rigidly connected and perform: (a) transfer motion with carrier  $c$ , and (b) relative motion about carrier. The helix angles of pinions 2 and 3 are of the same directions (or hand) in order to reduce the axial load on carrier  $c$  transformed from the pinions.

Assume that face-gear 4 is fixed and the train is used as a planetary one. It follows from the kinematics of the train that

$$-\frac{\omega_1 - \omega_c}{\omega_c} = m_{12}^{(c)} \cdot m_{34}^{(c)} = (-1) \frac{N_2}{N_1} (-1) \frac{N_4}{N_3} \quad (2.1)$$

Then, we obtain

$$m_{c1}^{(4)} = \frac{\omega_c}{\omega_1} = \frac{1}{1 - \frac{N_2 N_4}{N_1 N_3}} = \frac{N_1 N_3}{N_1 N_3 - N_2 N_4} \quad (2.2)$$

Here:  $\omega_c$  and  $\omega_1$  are the angular velocities of rotation of carrier  $c$  and face-gear 1;  $m_{c1}^{(4)}$  is the gear ratio of the train where carrier  $c$  and face-gear 1 are the driving and the driven members of the gear train and gear 4 is held at rest;  $N_i$  ( $i=1,2,3,4$ ) is the number of teeth.

In the case where  $N_2 = N_3$ , we obtain that

$$m_{c1}^{(4)} = \frac{N_1}{N_1 - N_4} \quad (2.3)$$

A substantial reduction of angular velocity  $\omega_c$  may be obtained. However, the efficiency of the train depends substantially on the applied gear ratio  $m_{c1}^{(4)}$ .

The gear train may be applied as well as a differential considering that the driving link is the carrier and the two driven members are 1 and 4. The advantage of such a differential is that zones of meshing (between 2 and 1, between 3 and 4) are separated and this permits increasing the precision and conditions of contact. The disadvantage (in comparison with a differential formed by bevel gears) is that only two planet gears may be applied and therefore it will limit the applied load. The advantage is the more simple technology of the train, and a higher precision obtained by grinding of gears and reduction of transmission errors (see section 2.2).

**Numerical Example 2.1.** The gear train of Figure 2.1 is formed as follows: output gear  $N_1 = 100$ , planet gears  $N_2 = N_3 = 7$ , fixed gear  $N_4 = 88$ , crossing angle  $\gamma = 75^\circ$ , helix angle  $\beta = 10^\circ$ . From equation (2.3) it follows that

$$m_{c1}^{(4)} = \frac{\omega_c}{\omega_1} = \frac{100}{100 - 88} = 8.333 \quad (2.4)$$

For such a gear drive, we may expect an efficiency of about 77.5 percent, computed considering a power loss of 2 percent at each gear mesh.

## 2.2 Tooth Contact Analysis (TCA)

The purpose of TCA is investigation of influence of errors of alignment on the transmission errors and what possibility exist for reduction of transmission errors.

TCA has been applied for a gear drive with parameters represented in Table 2.1. However, the approach applied is a general one and may be applied for the developed gear train with other input parameters.

The input member in the planetary gear drive is carrier  $c$  and the output gear is the face gear 1. The face gear 4 is considered as fixed. The respective inverted train is considered wherein the input gear is face gear 4, the output gear is face gear 1, and the carrier is fixed. The to-be-obtained function of transmission errors  $\Delta\phi_{14}$  will be the same as the function of transmission errors  $\Delta\phi_{1c}$  in the planetary gear drive.

The inverted gear train is a two-stage gear drive. Two gear mesh areas have to be considered: (1) one between face gear 4 and planet gear 3, and (2) another one between planet gear 2 and face gear 1. There are two sub-gear drives corresponding to those two areas of meshing, respectively, sub-gear drives (1) and (2).

An important parameter of design in a two-stage gear drive is the relative angle  $\delta$  of installation of the two gears that belong to the intermediate axis and that is used for reduction of the integrated function of transmission errors (see below). Figure 2.2 shows the relative angle  $\delta$  between planet gears 2 and 3 that is chosen initially as  $\delta = \pi/17$  rad. Since planet gears 2 and 3 are rigidly connected after installation of angle  $\delta$ , angles of rotation  $\phi_3$  and  $\phi_2$  are equal to each other. For the purpose of simplification, it is noted that  $\phi_3 = \phi_2 = \phi_p$ , wherein  $\phi_p$  is the angle of rotation of the axis that holds the planet gears.

Both sub-gear drives that constitute the two-stage gear drive are provided with a parabolic function of transmission errors. The theoretical gear ratio in each sub-gear drive is one. It is very important to determine the exact values of angles of rotation corresponding to the transition of one cycle of meshing to another in each sub-gear drive.

Determination of angles of transition of one cycle of meshing to another one in sub-gear drive 1 requires application of the following system of equations

$$\mathbf{r}_f^{(4)}(u_4, \theta_4, \phi_4) = \mathbf{r}_f^{(3)}(u_3, \theta_3, \phi_p) \quad (2.5)$$

$$\mathbf{n}_f^{(4)}(u_4, \theta_4, \phi_4) = \mathbf{n}_f^{(3)}(u_3, \theta_3, \phi_p) \quad (2.6)$$

$$\mathbf{r}_f^{(4)}(u_4', \theta_4', \phi_4 \pm \frac{\pi}{N_4}) = \mathbf{r}_f^{(3)}(u_3', \theta_3', \phi_p \pm \frac{\pi}{N_3}) \quad (2.7)$$

$$\mathbf{n}_f^{(4)}(u_4', \theta_4', \phi_4 \pm \frac{\pi}{N_4}) = \mathbf{n}_f^{(3)}(u_3', \theta_3', \phi_p \pm \frac{\pi}{N_3}) \quad (2.8)$$

Here, the plus sign is applied when the simultaneous contact of the current contacting pair and the forward contacting pair is considered, wherein the minus sign is applied when simultaneous contact of the current contacting pair and the backward contacting pair is considered. There are 10 unknowns and 10 equations that allow to determine  $\phi_{4\min}$  and  $\phi_{p\min}$  when the plus sign is applied and  $\phi_{4\max}$  and  $\phi_{p\max}$  when the minus sign is applied.

In the same way, angles of transition of one cycle of meshing to another in sub-gear drive 2 requires application of the following system of equations

$$\mathbf{r}_f^{(2)}(u_2, \theta_2, \phi_p) = \mathbf{r}_f^{(1)}(u_1, \theta_1, \phi_1) \quad (2.9)$$

$$\mathbf{n}_f^{(2)}(u_2, \theta_2, \phi_p) = \mathbf{n}_f^{(1)}(u_1, \theta_1, \phi_1) \quad (2.10)$$

$$\mathbf{r}_f^{(2)}\left(u_2', \theta_2', \phi_p \pm \frac{\pi}{N_2}\right) = \mathbf{r}_f^{(1)}\left(u_1', \theta_1', \phi_1 \pm \frac{\pi}{N_1}\right) \quad (2.11)$$

$$\mathbf{n}_f^{(2)}\left(u_2', \theta_2', \phi_p \pm \frac{\pi}{N_2}\right) = \mathbf{n}_f^{(1)}\left(u_1', \theta_1', \phi_1 \pm \frac{\pi}{N_1}\right) \quad (2.12)$$

that allows  $\phi_{pmin}^*$  to be determined when simultaneous contact of the current and the forward pairs of teeth is considered and  $\phi_{pmax}^*$  when the current and the backward pairs of contacting teeth are simultaneously in contact.

The procedure to determine angles  $\phi_4$ ,  $\phi_p$ , and  $\phi_1$ , is as follows:

Step 1. Angle  $\phi_4$  is considered as an input value and is chosen inside the interval  $[\phi_{4min}, \phi_{4max}]$ .

Step 2. Point of contact between gear tooth surfaces 4 and 3 and angle  $\phi_p$  are obtained from the solution of system equations (2.5) to (2.6)

$$\mathbf{r}_f^{(4)}(u_4, \theta_4, \phi_4) = \mathbf{r}_f^{(3)}(u_3, \theta_3, \phi_p)$$

$$\mathbf{n}_f^{(4)}(u_4, \theta_4, \phi_4) = \mathbf{n}_f^{(3)}(u_3, \theta_3, \phi_p)$$

The value of  $\phi_p$  will be inside the interval  $[\phi_{pmin}, \phi_{pmax}]$  since the value of  $\phi_4$  is inside the interval  $[\phi_{4min}, \phi_{4max}]$ .

Step 3. The following action depends on the value of angle  $\phi_p$ :

- (1)  $\phi_p < \phi_{pmin}^*$ . In this case the forward pair of teeth of gears 2 and 1 is in contact and the system of equations is given by

$$\mathbf{r}_f^{(2)}\left(u_2, \theta_2, \phi_p + \frac{\pi}{N_2}\right) = \mathbf{r}_f^{(1)}\left(u_1, \theta_1, \phi_1 + \frac{\pi}{N_1}\right) \quad (2.13)$$

$$\mathbf{n}_f^{(2)}\left(u_2, \theta_2, \phi_p + \frac{\pi}{N_2}\right) = \mathbf{n}_f^{(1)}\left(u_1, \theta_1, \phi_1 + \frac{\pi}{N_1}\right) \quad (2.14)$$

- (2)  $\phi_{pmin}^* < \phi_p < \phi_{pmax}^*$ . In this case the middle pair of teeth of gears 2 and 1 is in contact and the system of equations is given by

$$\mathbf{r}_f^{(2)}(u_2, \theta_2, \phi_p) = \mathbf{r}_f^{(1)}(u_1, \theta_1, \phi_1)$$

$$\mathbf{n}_f^{(2)}(u_2, \theta_2, \phi_p) = \mathbf{n}_f^{(1)}(u_1, \theta_1, \phi_1)$$

- (3)  $\phi_p > \phi_{pmax}^*$ . In this case the backward pair of teeth of gears 2 and 1 is in contact and the system of equations is given by

$$\mathbf{r}_f^{(2)}(u_2, \theta_2, \phi_p - \frac{\pi}{N_2}) = \mathbf{r}_f^{(1)}(u_1, \theta_1, \phi_1 - \frac{\pi}{N_1}) \quad (2.15)$$

$$\mathbf{n}_f^{(2)}(u_2, \theta_2, \phi_p - \frac{\pi}{N_2}) = \mathbf{n}_f^{(1)}(u_1, \theta_1, \phi_1 - \frac{\pi}{N_1}) \quad (2.16)$$

Solution of the corresponding system of equations allows angle  $\phi_1$  to be determined.

Step 4. Another value of  $\phi_4$  inside the interval  $[\phi_{4min}, \phi_{4max}]$  is considered and steps from 1 to 3 are repeated.

Figure 2.3 shows the functions of transmission errors that correspond to sub-gear drives 1 and 2. Figure 2.4 shows the resulting function of transmission errors  $\Delta\phi_{14}$  when three cycles of meshing are considered. The drawings show that two parabolic branches exist in each cycle of meshing. One of the branches corresponds to the contact of the middle pair of teeth (relation  $\phi_{pmin}^* < \phi_p < \phi_{pmax}^*$  is satisfied) and the other branch corresponds to the contact of the backward pair of teeth (relation  $\phi_p > \phi_{pmax}^*$  is satisfied). These results have been obtained considering an installation angle  $\delta = \pi/17$  rad.

Figure 2.5 shows the paths of contact on each tooth surface.

Figure 2.6 shows the resulting function of transmission errors  $\Delta\phi_{14}$  for different values of installation angle  $\delta$ . These results confirm the following: the relative size of the parabolic branches and the maximum value of transmission error changes with  $\delta$ , although the functions of transmission errors between gears 4 and 3, and between gears 2 and 1 (Fig. 2.3) have not been changed.

Figure 2.7 shows two cases of interest. Figure 2.7(a) shows the case wherein just one parabolic branch is obtained. In this case the installation angle was

$$\delta = \frac{\pi}{17} + \phi_{pmax} - \phi_{pmax}^* = \frac{\pi}{17} - 0.134658 \text{ rad}$$

Figure 2.7(b) shows the case wherein the two parabolic branches are of the same size. In this case the installation angle was  $\delta = \pi/17 + 0.0518$  rad. The maximum value of transmission errors that it could be obtained for all cases of  $\delta$  was the one obtained in Fig. 2.7(a) (22 arcsec) while the minimum value for all cases of  $\delta$  was the obtained in Fig. 2.7(b) (6 arcsec).

Similar results are obtained when the planetary gear drive works as a multiplier with face gear 4 as the output member and carrier c as the input member. The integrated function of transmission errors  $\Delta\phi_{4c}$  wherein face gear 1 is fixed is the same as the function  $\Delta\phi_{41}$  of the respective inverted gear train.

Figure 2.8 shows the integrated function of transmission errors for an installation angle  $\delta = \pi/17$  rad.

Figures 2.9(a) and (b) show two particular cases that correspond to installation angles  $\delta = \pi/17 - 0.134658$  rad and  $\delta = \pi/17 + 0.0518$  rad.

## 2.3 Conclusions

The obtained results allow the following conclusions to be drawn:

(1) Profile crowning of face and planet gears that form the planetary gear drive can obtain a longitudinal path of contact and a pre-design and parabolic function of transmission errors at each gear mesh. Edge contact has been avoided.

(2) The integrated function of transmission errors has been obtained considering at each instant the pair of teeth that is meshing. A function based on two branches of parabolic type has been obtained.

(3) The level of transmission errors and the size of parabolic branches of the integrated function of transmission errors may be modified through installation angle  $\delta$  between planet gears. An optimized value of  $\delta$  may be obtained for reducing the level of transmission errors of the integrated function of transmission errors.

## References

1. F.L. Litvin, A. Fuentes, I. Gonzalez-Perez, A. Piscopo, and P. Ruzziconi, *Face Gear Drive With Helical Involute Pinion: Geometry, Generation by a Shaper and a Worm, Avoidance of Singularities and Stress Analysis*, NASA/CR—2005-213443, 2005.
2. F.L. Litvin, and A. Fuentes, *Gear Geometry and Applied Theory*, Second Edition. Cambridge University Press, New York, 2004.
3. G.A. Korn, and T.M. Korn, *Mathematics Handbook for Scientist and Engineers*, McGraw-Hill, Inc., 2nd Ed., 1968.
4. Visual Numerics Inc., IMSL Fortran 90 MP Library, v. 3.0, info@boulder.vni.com, 1998.
5. F.L. Litvin, A. Fuentes, C. Zanzi, P. Matteo, and F.R. Handschuh, *Design, Generation and Stress Analysis of Two Versions of Geometry of Face-Gear Drives*, Mechanism and Machine Theory 37, pp. 1179–1211, 2002.
6. F.L. Litvin, A. Fuentes, I. Gonzalez-Perez, L. Carnevali, K. Kawasaki, R.F. Handschuh, *Modified Involute Helical Gears: Computerized Design, Simulation of Meshing and Stress Analysis*. Computer Methods in Applied Mechanics and Engineering, Vol. 192, pp. 3619–3655, 2003.

TABLE 2.1.—PLANETARY GEAR TRAIN DATA

| Design parameters                              |                        |
|--|------------------------|
| Number of teeth of face gear 1, $N_1$          | 100                    |
| Number of teeth of planet gear 2, $N_2$        | 17                     |
| Number of teeth of planet gear 3, $N_3$        | 17                     |
| Number of teeth of face gear 4, $N_4$          | 88                     |
| Number of teeth of the shaper, $N_s$           | 20                     |
| Module, $m$                                    | 5.0 mm                 |
| Pressure angle, $\alpha$                       | 20°                    |
| Helix angle, $\beta$                           | 10°                    |
| Shaft angle, $\gamma$                          | 75°                    |
| Profile crowning coefficients for planet gears | 0.001 mm <sup>-1</sup> |
| Profile crowning coefficients for face gears   | 0.002 mm <sup>-1</sup> |

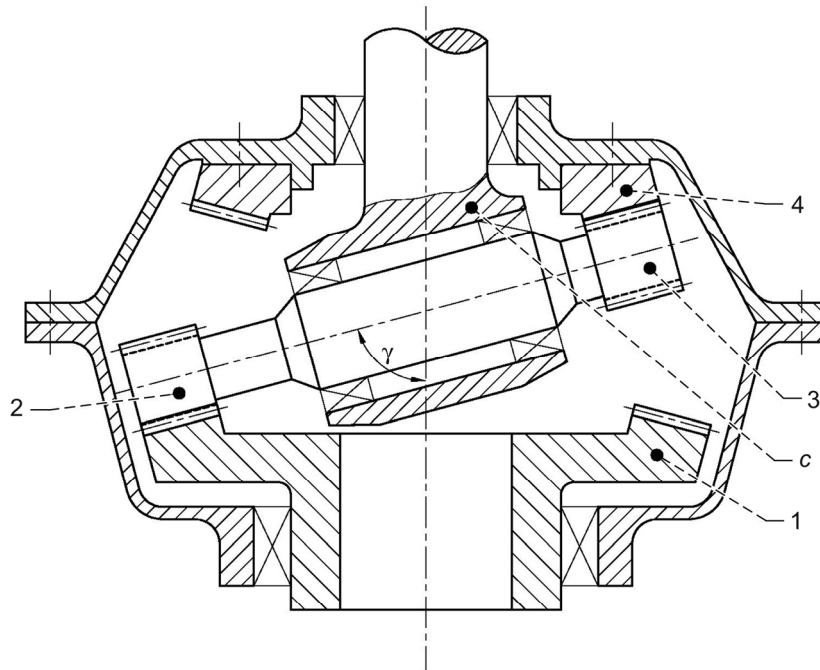


Figure 2.1.—Planetary face gear drive.

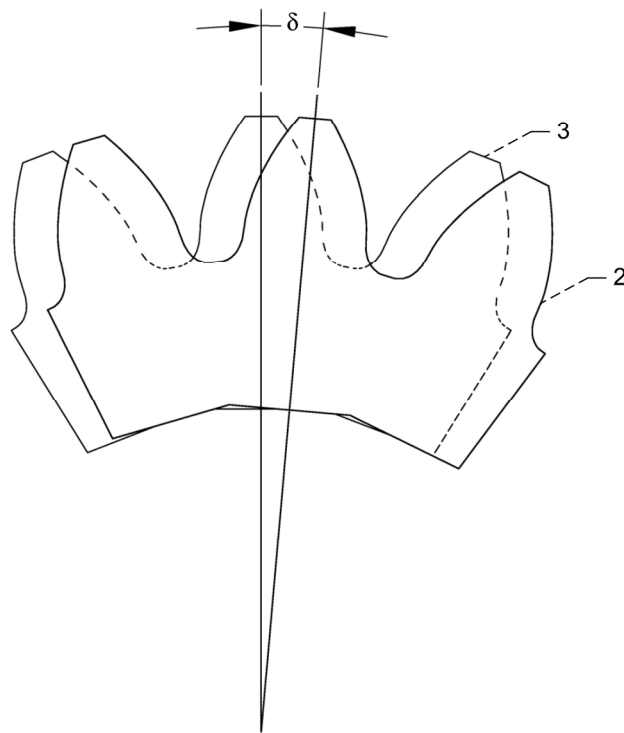


Figure 2.2.—Installation angle between planet gears 2 and 3.

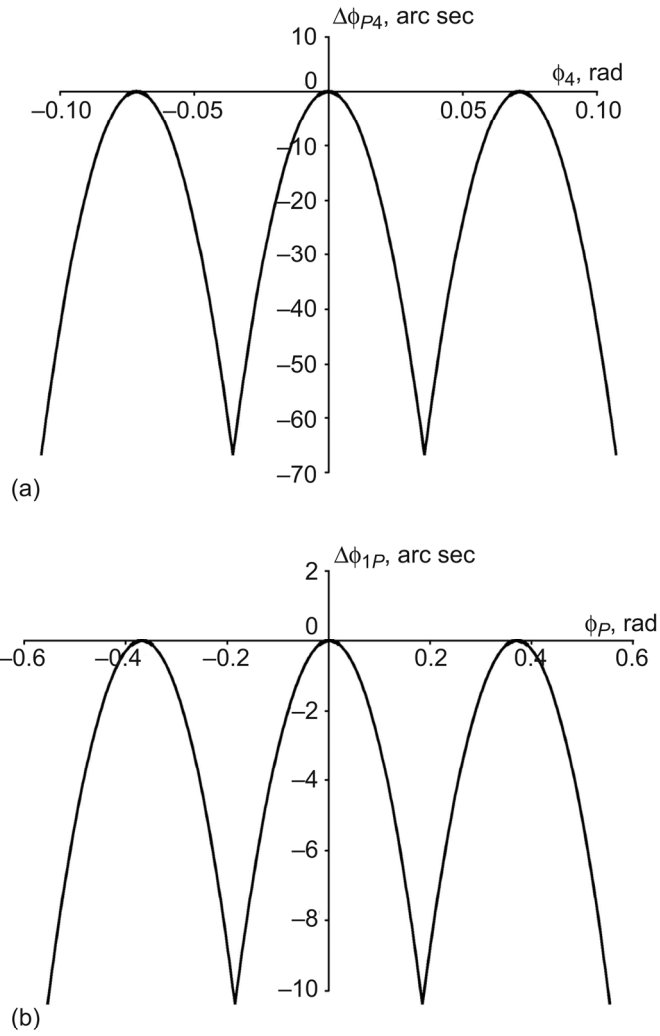


Figure 2.3.—Functions of transmission errors. (a) Between face gear 4 and planet gear 3. (b) Between planet gear 2 and face gear 1.

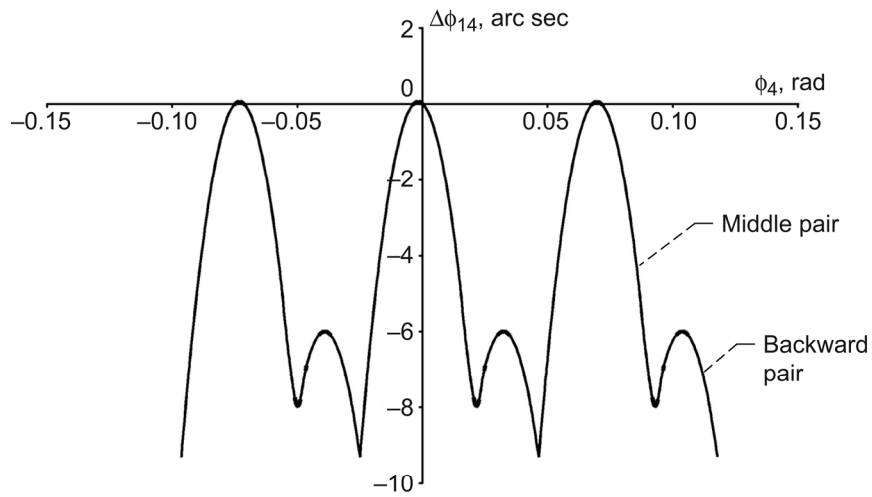


Figure 2.4.—Resulting functions of transmission errors  $\Delta\phi_{14}$  based on two parabolic branches for each cycle of meshing.

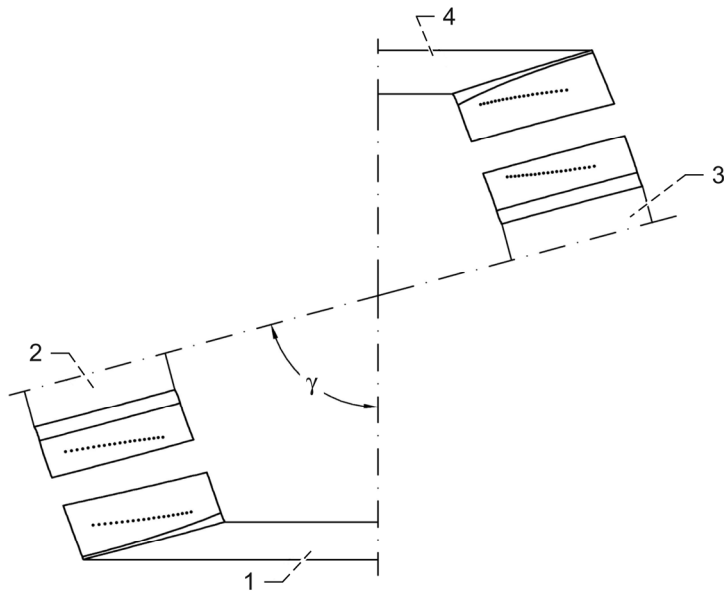


Figure 2.5.—Paths of contact when no errors of alignment are considered.

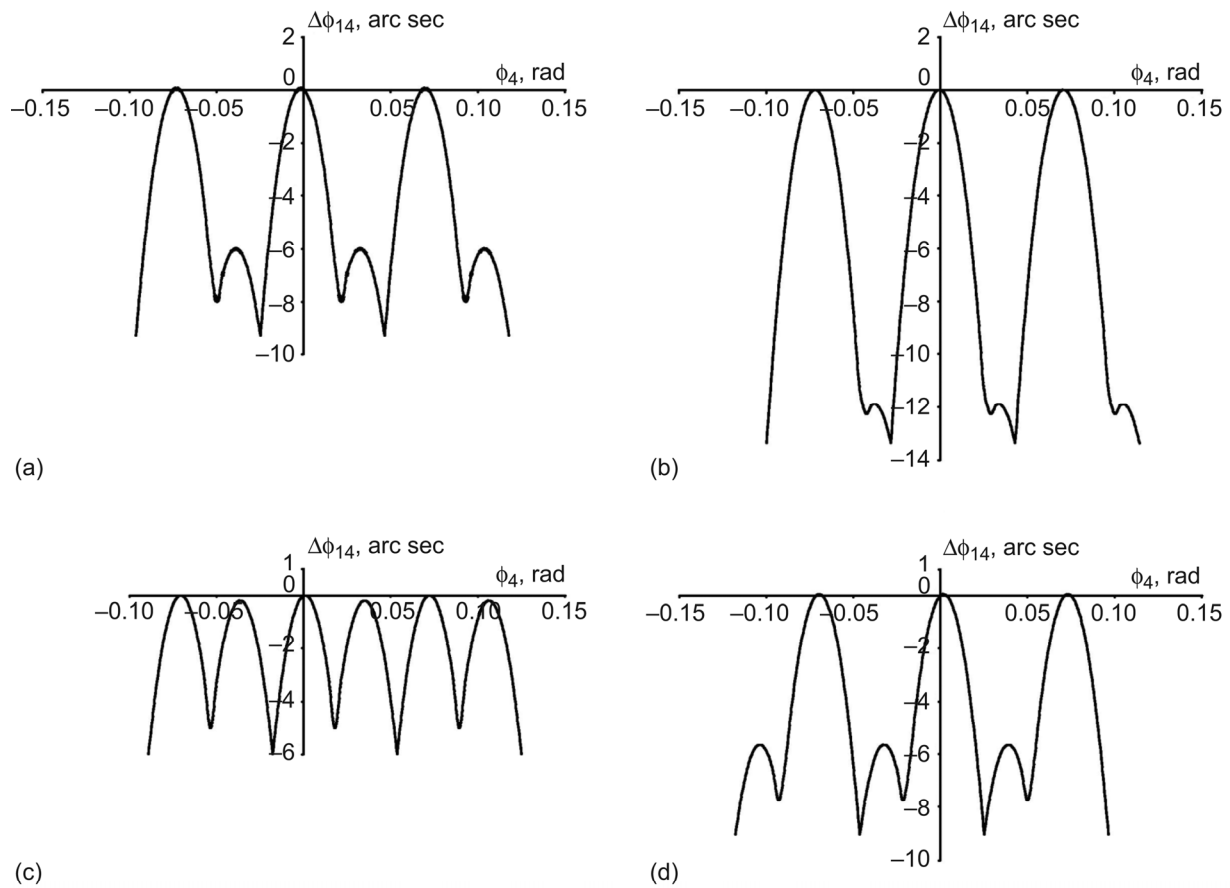


Figure 2.6.—Resulting functions of transmission errors  $\Delta\phi_{14}$  for different values of installation angle  $\delta$ . (a)  $\delta = \pi/17$  rad. (b)  $\delta = \pi/17 - 0.05$  rad. (c)  $\delta = \pi/17 + 0.05$  rad. (d)  $\delta = \pi/17 + 0.1$  rad.

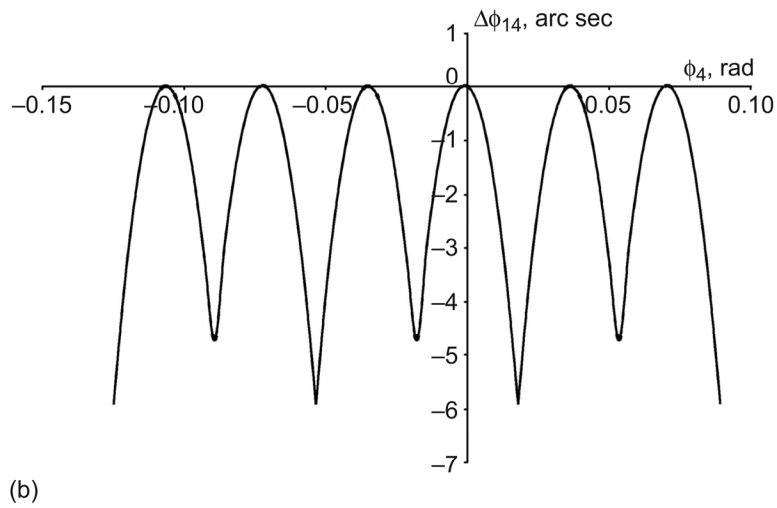
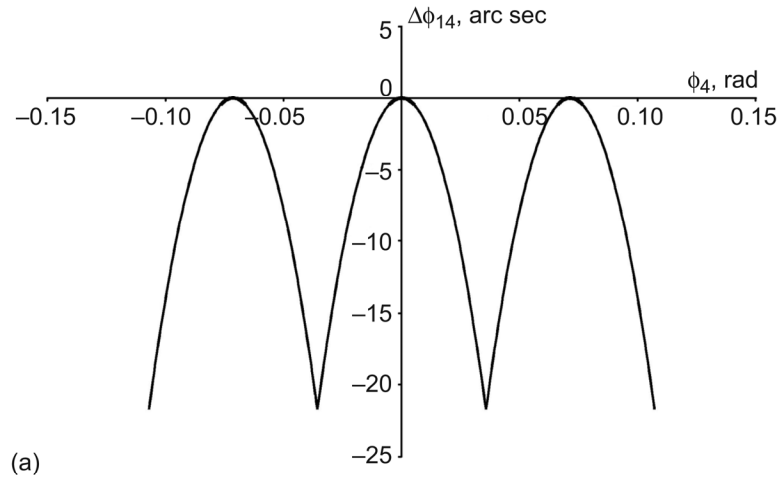


Figure 2.7.—Resulting functions of transmission errors  $\Delta\phi_{14}$  for particular cases. (a)  $\delta = \pi/17 - 0.134658$  rad. (b)  $\delta = \pi/17 + 0.0518$  rad.

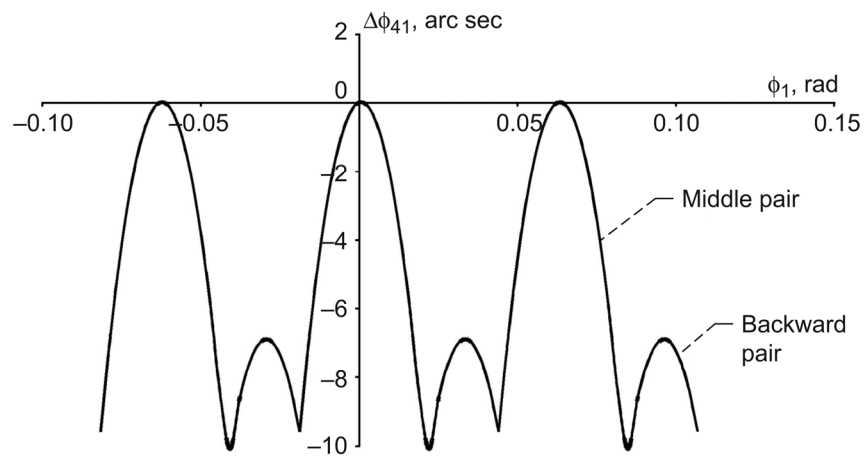


Figure 2.8.—Resulting function of transmission errors  $\Delta\phi_{14}$  based on two parabolic branches for each cycle of meshing for the case of the planetary face gear drive working as a multiplier (speed increaser).

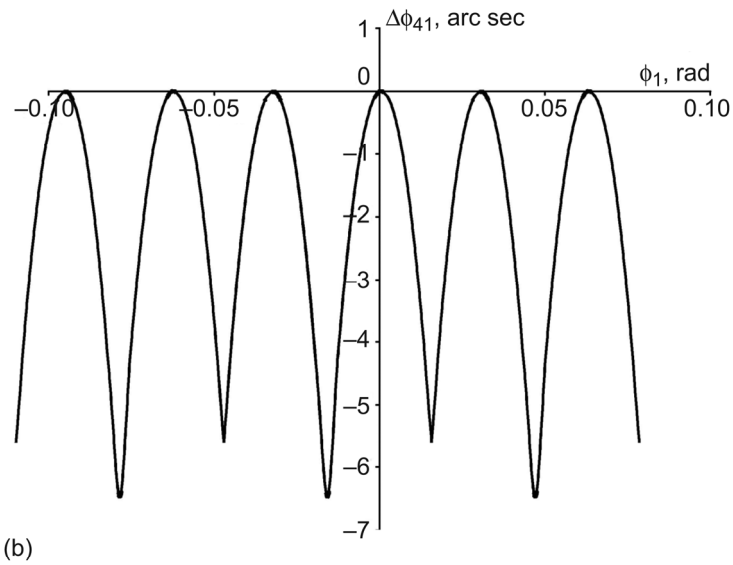
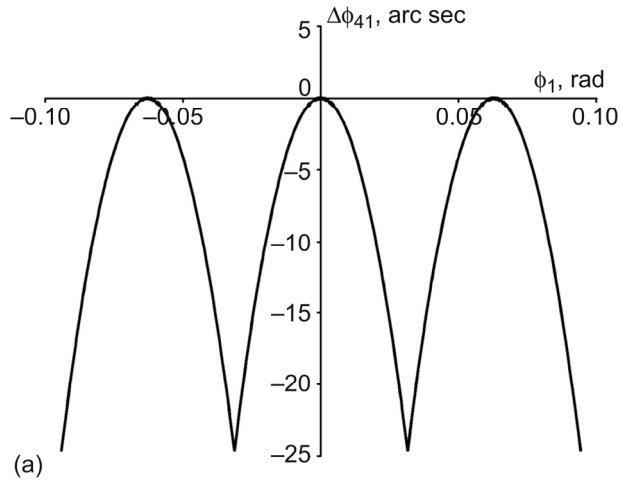


Figure 2.9.—Resulting functions of transmission errors  $\Delta\phi_{41}$  in a planetary face gear drive working as a multiplier (speed increaser) for particular cases. (a)  $\delta = \pi/17 - 0.134658$  rad. (b)  $\delta = \pi/17 + 0.0518$  rad.

## Part 3.—Design and Simulation of an Isostatic Planetary Gear Train

### 3.1 Introduction

A planetary gear train formed by a sun gear (1), several planets (2) all mounted on carrier  $c$ , and an internal ring gear (3) is considered. Such a multi-body mechanism may cause uneven load distribution between the planets (Ref. 1). The approach of *regulation* has been proposed in order to improve load distribution (see Part 1).

An alternative approach, although less general, is now represented. The approach is based on the concept of an isostatic gear train. By definition, in an isostatic mechanism the number of constrains equals the number of degrees of freedom. It follows that the configuration (the status) of the mechanism may be determined univocally.

The contents of this part of the report cover:

Determination of the conditions of design for obtaining an isostatic planetary gear.

Formulation of algorithms for simulation of conditions of meshing of such mechanism.

Development of a computer program based on algorithms described later. Development of a numerical example confirms: (a) validation of proposed approach, and (b) investigation of effect of possible errors of manufacturing and assembly.

### 2.2 Static Analysis

**Degrees of Freedom.** The mechanism is considered as a planar one with 3 degrees of freedom (DOF) for each rigid body: two and one, for translational and rotational motions, respectively. The total number of DOF is computed as follows

| Member      | DOF      |
|-------------|----------|
| Sun         | 3        |
| Planets     | $3N_p$   |
| Carrier     | 3        |
| Ring        | 3        |
| Total $N_f$ | $9+3N_p$ |

where  $N_p$  is the number of planet gears.

**Case 1 constraints.** In case 1 we consider the following:

- (i) Axis of rotation of the sun is fixed. Considered as given.
- (ii) Angular position  $\phi_1$  of the sun gear is considered as given.
- (iii) Axis of rotation of the carrier is fixed. Considered as given.
- (iv) Axis and angular position of the ring gear are considered as given.
- (v) Each planet gear is pinned rigidly connected to the carrier.
- (vi) Each planet gear is in tangency (contact) with the sun and ring gears, respectively.

Based on the above requirements, the total number of constrains  $N_c$  is determined as follows

| Condition   | Constrains |
|-------------|------------|
| (i)         | 2          |
| (ii)        | 1          |
| (iii)       | 2          |
| (iv)        | 3          |
| (v)         | $2N_p$     |
| (vi)        | $2N_p$     |
| Total $N_c$ | $9+3N_p$   |

Equalling the available degrees of freedom with the imposed constrains, we obtain the following equation

$$9 + 3N_p = 8 + 4N_p \quad (3.1)$$

It follows that this mechanism is isostatic for  $N_p = 1$ .

**Case 2 constraints.** Our goal is to reduce the number of constrains in order to obtain an isostatic gear train with  $N_p > 1$  planet gears. In case 2 we consider:

- (i) axis of rotation of the sun is free, not constrained
- (ii) angular position of the sun  $\phi_1$  is given
- (iii) axis of rotation of the carrier is fixed, given
- (iv) axis and angular position of the ring gear are given
- (v) each planet gear is pinned to the carrier
- (vi) each planet gear is in tangency (contact) with the sun and ring gears

Based on the above requirements, the total number of constrains  $N_c$  is determined as follows

| Condition   | Constrains |
|-------------|------------|
| (i)         | 0          |
| (ii)        | 1          |
| (iii)       | 2          |
| (iv)        | 3          |
| (v)         | $2N_p$     |
| (vi)        | $2N_p$     |
| Total $N_c$ | $6+4N_p$   |

Equalling the available degrees of freedom with the imposed constrains, we obtain the following equation

$$9 + 3N_p = 6 + 4N_p \quad (3.2)$$

It follows that this mechanism is isostatic for  $N_p = 3$  planet gears.

**Case 3 constraints.** The number of constraints may be further reduced making free the location of the center position of the carrier. In case 3 we consider the following:

- (i) axis of rotation of the sun gear is free, not constrained
- (ii) angular position  $\phi_1$  of sun gear is given
- (iii) axis of rotation of the carrier is free, not constrained
- (iv) axis and angular position of the ring gear are given.
- (v) each planet gear is pinned to the carrier
- (vi) each planet gear is in tangency (contact) with sun and ring gears

Based on the above requirements, the total number of constrains  $N_c$  is determined as follows

| Condition   | Constrains |
|-------------|------------|
| (i)         | 0          |
| (ii)        | 1          |
| (iii)       | 0          |
| (iv)        | 3          |
| (v)         | $2N_p$     |
| (vi)        | $2N_p$     |
| Total $N_c$ | $4+4N_p$   |

Equalling the available degrees of freedom with the imposed constrains, we obtain the following equation

$$9 + 3N_p = 4 + 4N_p \quad (3.3)$$

It follows that this mechanism is isostatic for  $N_p = 5$  planet gears.

**Note 1.** At least one member of the gear drive (sun/ring/carrier) has to be fully constrained (to be grounded), since the position of the mechanism has to be defined with respect to a fixed reference system.

**Note 2.** One may chose to free the location of the center of the ring instead of the center of the sun, etc.

**Note 3.** It follows that it is not possible to define an isostatic planetary gear train with more than five planets, unless the condition of *pinning* of planets on the carrier is removed. However, this case is not considered in this report.

### 3.3 Simulation of Contact

**Introduction.** Simulation of contact of such a mechanism is based on the well known procedure of tooth contact analysis (TCA) (Ref. 2). The main differences are as follows:

(i) Unlike to a conventional procedure of TCA, the simulation of meshing should not be limited only to a pair of contacting teeth. The angle of the driving link may perform much more than a single cycle of meshing, therefore the algorithm of simulation has to provide automatically which of the contact pairs is actually in mesh.

(ii) The mechanism may include several pairs of gears. Therefore, tangency of several couples of surfaces has to be considered at each step.

(iii) The axes of the gears may be fixed or be free, as in the case of planetary trains. In this case, unknowns of the system of equations will include the coordinates identifying positions of the axes.

To comply with the requirement (i), the following steps have to be considered:

- (1) Starting from a reference tooth, all teeth of each gear have to be numbered, see Figure 3.2. The direction of indexes has to be related with the direction of rotation of the gear: for instance, the tooth that will be in meshing after tooth index 0 will be  $-1$  or  $1$ , depending on the direction of rotation.
- (2) An initial configuration of the mechanism is considered. For each pair of contacting teeth, respective pair of contacting indexes have to be provided. This can be done either manually or automatically, by a subroutine.
- (3) A new angular position of the driving link (slightly changed from the one used in the previous step) is provided. TCA is performed to the same pair of teeth that was in mesh at the step before. In addition, the next pair of teeth is verified for determination of backlash (see below). If the backlash is negative, this means that interference is occurring, therefore this pair of teeth is actually meshing. At this point, the indexes of contacting pair of teeth have to be updated, and TCA repeated for the new contacting pair.

The objective of this research is simulation of meshing of the isostatic planetary gear train, and an investigation of the effects of various errors that may affect such a mechanism.

In the following paragraphs, explanations of all the steps necessary for performing such a simulation are provided. The steps are:

- (a) Determination of equations of gear tooth surfaces represented in the fixed reference system.
- (b) Formulation of algorithms for tangency of surfaces and determination of backlash.
- (c) Application of above algorithms for analysis of the whole gear train. A large set of non-linear equations is obtained. Numerical solution of such a system of equations has proven to be very complicated and requires almost-exact guess values. A method that allows substantial simplification of the problem to be solved is proposed. The method is based on application of additional (*fictitious*) unknowns permitting it break down of the full set of equations in several simpler sets, that are easier to solve.

A computer program based on the ideas described above has been developed. The computer program has been applied for simulation of various errors of manufacturing and installment of the gear drive with three planets, case 2. Results are represented and commented in the contents of the numerical example.

### 3.3.1 Equations of Gear Tooth Surfaces

Equations of gear tooth surfaces are derived in accordance to the methods described in Reference 2. Geometry of spur and helical gears are described as well in Reference 4.

**Sun Gear Tooth Surface.** The surface of the sun gear is a regular involute helical surface, represented in  $S_1$  in two parameter form as

$$\mathbf{r}_1^{(1)}(u^{(1)}, \theta^{(1)}) \quad (3.4)$$

We assume that (3.4) represents the surface of the reference tooth, with index  $i_s^i = 0$ . Here,  $i_s$  designates an index of the sun gear, and superscript  $i = 1, \dots, 5$  designates the tooth that is in mesh with the  $i^{\text{th}}$  planet. Equations of other teeth are represented in  $S_1$  as

$$\mathbf{r}_1^{(1)}(u^{(1)}, \theta^{(1)}, i_s^i) = \mathbf{M}_1(i_s^i) \mathbf{r}_1^{(1)}(u^{(1)}, \theta^{(1)}) \quad (3.5)$$

where

$$\mathbf{M}_1(i_s^i) = \begin{pmatrix} \cos q & \sin q & 0.0 & \varepsilon^{(1)} \\ -\sin q & \cos q & 0.0 & 0.0 \\ 0.0 & 0.0 & 1.0 & 0.0 \\ 0.0 & 0.0 & 0.0 & 1.0 \end{pmatrix} \quad (3.6)$$

and  $q = (2\pi / N^{(1)})i_s^i$ . Here,  $\varepsilon^{(1)}$  represents the *runout error* of the gear and the bearings, in other words the error of eccentricity of rotation of the gear teeth.

The surface is represented in the fixed reference system  $S_f$  by the following matrix of transformation

$$\mathbf{M}_{f1}(\phi^{(1)}, E_x^{(1)}, E_y^{(1)}) = \begin{pmatrix} \cos \phi^{(1)} & -\sin \phi^{(1)} & 0.0 & \Delta E_x^{(1)} \\ \sin \phi^{(1)} & \cos \phi^{(1)} & 0.0 & \Delta E_y^{(1)} \\ 0.0 & 0.0 & 1.0 & 0.0 \\ 0.0 & 0.0 & 0.0 & 1.0 \end{pmatrix} \quad (3.7)$$

$$\mathbf{r}_1^{(1)}(u^{(1)}, \theta^{(1)}, E_x^{(1)}, E_y^{(1)}, i_s^1) = \mathbf{M}_{f1}(\phi^{(1)}, \Delta E_x^{(1)}, \Delta E_y^{(1)}) \mathbf{M}_1(i_s^1) \mathbf{r}_1^{(1)}(u^{(1)}, \theta^{(1)}) \quad (3.8)$$

Here,  $\Delta E_x^{(1)}$  and  $\Delta E_y^{(1)}$  may play two different roles: in the case wherein the position of the sun gear is given, they represent the predetermined errors of installment. Else, in the case where the axis of the sun gear is free, they represent as well the unknowns of the problem. Parameter  $\phi_1$  represents the input of the linkage, and is given in any case.

**Planet Gear Tooth Surface.** The surface of the planetary gear is a modified double-crowned surface (Ref. 3), represented in  $S_2$  in four parametric form as

$$\mathbf{r}_2^{(2,i)}(u^{(2,i)}, \theta^{(2,i)}, \psi^{(2,i)}, \lambda^{(2,i)}) \quad (3.9)$$

$$f_1(u^{(2,i)}, \theta^{(2,i)}, \psi^{(2,i)}, \lambda^{(2,i)}) = 0 \quad (3.10)$$

$$f_2(u^{(2,i)}, \theta^{(2,i)}, \psi^{(2,i)}, \lambda^{(2,i)}) = 0 \quad (3.11)$$

Here,  $f_1$  and  $f_2$  are the equations of meshing.

Teeth numbering and gear run-out errors are modelled similarly as in Equations (3.5) and (3.6). Tooth indexes  $i_{ps}^i$  and  $i_{pr}^i$ , respectively, designate the tooth of the  $i^{th}$  planet, being in meshing with the sun and the ring gears.

The motion of the planetary gear with respect to the fixed reference system is described by the following two matrices of transformation

$$\mathbf{M}_{c2(i)}(\phi^{(2,i)}) = \begin{pmatrix} \cos \phi^{(2,i)} & -\sin \phi^{(2,i)} & 0.0 & r_c + \Delta r_c^{(2,i)} \\ \sin \phi^{(2,i)} & \cos \phi^{(2,i)} & 0.0 & \Delta E_t^{(2,i)} \\ 0.0 & 0.0 & 1.0 & 0.0 \\ 0.0 & 0.0 & 0.0 & 1.0 \end{pmatrix} \quad (3.12)$$

$$\mathbf{M}_{fc}(\phi^{(c)}, \Delta E_x^{(c)}, \Delta E_y^{(c)}) = \begin{pmatrix} \cos q_c & -\sin q_c & 0.0 & \Delta E_x^{(c)} \\ \sin q_c & \cos q_c & 0.0 & \Delta E_y^{(c)} \\ 0.0 & 0.0 & 1.0 & 0.0 \\ 0.0 & 0.0 & 0.0 & 1.0 \end{pmatrix} \quad (3.13)$$

where  $q_c = \phi^{(c)} + (2\pi / N_p)(i-1)$ ,  $N_p$  is the number of planet gears,  $i = 1, \dots, 5$  is the index of the considered planet gear. Here,  $\Delta r_c$  represents the error of installment of the planet gear measured in radial direction, and  $r_c$  is the radius of the carrier. Value  $\Delta E_t$  represents the error of indexing of the carrier in tangential direction. Parameter  $\phi^{(2,i)}$  represents the angle of rotation of the  $i^{th}$  planet with respect to the carrier, and is an unknown.

Similarly as in the case of the sun gear, parameters  $\Delta E_x^{(c)}$  and  $\Delta E_y^{(c)}$ , may be considered as given data or as unknowns that represent the errors of installment of the carrier on the fixed reference system.

The surface is represented in the fixed reference system by the following matrix of transformation

$$\mathbf{r}^{(2,i)}(u^{(2,i)}, \theta^{(2,i)}, \psi^{(2,i)}, \lambda^{(2,i)}, \phi^{(c)}, E_x^{(c)}, E_y^{(c)}, \phi^{(2,i)}, i_p) = \mathbf{M}_{fc}(\phi^{(c)}, \Delta E_x^{(c)}, \Delta E_y^{(c)}) \mathbf{M}_{c2(i)}(\phi^{(2,i)}) \mathbf{M}_2^{(2,i)}(i_p) \mathbf{r}_2^{(2,i)}(u^{(2,i)}, \theta^{(2,i)}, \psi^{(2,i)}, \lambda^{(2,i)}) \quad (3.14)$$

Parameters  $\phi^{(c)}$  and  $\phi^{(2,i)}$  are unknowns.

**Ring Gear Tooth Surface.** The surface of the ring gear is a regular involute-helical surface, represented in  $S_3$  in two parameter form as

$$\mathbf{r}_3^{(3)}(u^{(3)}, \theta^{(3)}) \quad (3.15)$$

Teeth numbering and gear run-out error are introduced similarly as in Equations (3.5) and (3.6). The index of the contacting teeth is designated by  $i_r^i$ , where superscript  $i = 1, \dots, 5$  identifies the considered planet gear.

The surface is represented in the fixed reference system by the following matrix of transformation

$$\mathbf{M}_{f3} = \begin{pmatrix} 1.0 & 0.0 & 0.0 & 0.0 \\ 0.0 & 1.0 & 0.0 & 0.0 \\ 0.0 & 0.0 & 1.0 & 0.0 \\ 0.0 & 0.0 & 0.0 & 1.0 \end{pmatrix} \quad (3.16)$$

$$\mathbf{r}^{(3)}(u^{(3)}, \theta^{(3)}, i_r^i) = \mathbf{M}_{f3} \mathbf{M}_3(i_r^i) \mathbf{r}_3^{(3)}(u^{(3)}, \theta^{(3)}) \quad (3.17)$$

We remind that the gear is fixed in  $S_f$ .

### 3.3.2 Algorithms for Determination of Tangency and Backlash of Surfaces

For the analysis to be performed, it will be more convenient to consider the mechanism as a set of *subtrains*. A subtrain is constituted by: (1) the sun gear, (2) only one planetary gear, and (3) the ring gear.

**Equations of Tangency for a Subtrain.** The following represent the equations of tooth surfaces of tangency of the  $i^{th}$  subtrain.

$$\begin{aligned}
 & \mathbf{r}^{(1)}(u_i^{(1)}, \theta_i^{(1)}, \phi^{(1)}, i_s^i) - \mathbf{r}^{(2,i)}(u_s^{(2,i)}, \theta_s^{(2,i)}, \psi_s^{(2,i)}, \lambda_s^{(2,i)}, \phi^{(2,i)}, i_{ps}^i) = \mathbf{0} \\
 & \left( \frac{\partial \mathbf{r}^{(1)}}{\partial u_i^{(1)}} \times \frac{\partial \mathbf{r}^{(1)}}{\partial \theta_i^{(1)}} \right) \cdot \frac{\partial \mathbf{r}^{(2,i)}}{\partial u_s^{(2,i)}} = 0 \\
 & \left( \frac{\partial \mathbf{r}^{(1)}}{\partial u_i^{(1)}} \times \frac{\partial \mathbf{r}^{(1)}}{\partial \theta_i^{(1)}} \right) \cdot \frac{\partial \mathbf{r}^{(2,i)}}{\partial \theta_s^{(2,i)}} = 0 \\
 & f_1(u_s^{(2,i)}, \theta_s^{(2,i)}, \psi_s^{(2,i)}, \lambda_s^{(2,i)}) = 0 \\
 & f_2(u_s^{(2,i)}, \theta_s^{(2,i)}, \psi_s^{(2,i)}, \lambda_s^{(2,i)}) = 0 \tag{3.18} \\
 \\
 & \mathbf{r}^{(2,i)}(u_p^{(2,i)}, \theta_p^{(2,i)}, \psi_p^{(2,i)}, \lambda_p^{(2,i)}, \phi^{(c,i)}, \phi^{(2,i)}, i_{pr}^i) - \mathbf{r}^{(3)}(u_i^{(3)}, \theta_i^{(3)}, i_r^i) = \mathbf{0} \\
 & \left( \frac{\partial \mathbf{r}^{(3)}}{\partial u_i^{(3)}} \times \frac{\partial \mathbf{r}^{(3)}}{\partial \theta_i^{(3)}} \right) \cdot \frac{\partial \mathbf{r}^{(2,i)}}{\partial u_p^{(2,i)}} = 0 \\
 & \left( \frac{\partial \mathbf{r}^{(3)}}{\partial u_i^{(3)}} \times \frac{\partial \mathbf{r}^{(3)}}{\partial \theta_i^{(3)}} \right) \cdot \frac{\partial \mathbf{r}^{(2,i)}}{\partial \theta_p^{(2,i)}} = 0 \\
 & f_1(u_p^{(2,i)}, \theta_p^{(2,i)}, \psi_p^{(2,i)}, \lambda_p^{(2,i)}) = 0 \\
 & f_2(u_p^{(2,i)}, \theta_p^{(2,i)}, \psi_p^{(2,i)}, \lambda_p^{(2,i)}) = 0
 \end{aligned}$$

Here, angle  $\phi^{(c,i)}$  represents the angle of rotation of carrier of the  $i^{th}$  subtrain.

For formulation of Equation (3.18), it has been assumed that the centers of rotation of the sun gear and the carrier are given (parameters  $\Delta E$  do not appear here in the list of unknowns). The obtained set of non-linear Equation (3.18) includes 14 equations in 14 unknowns. Numerical solution of such a system may be performed with the Newton-Raphson method (Ref. 5). Determination of suitable guess values for solution is a complex problem, but it has been proven that system (3.18) is sufficiently stable.

**Determination of Backlash of Neighboring Tooth Surfaces.** As it has been previously explained, the determination of backlash of tooth surfaces neighboring to the contacting ones is the key for the detection of the change of meshing from one pair of teeth to the next one.

Analysis of backlash is performed after solution of system (3.18). Angular positions  $\phi^{(c,i)}$  and  $\phi^{(2,i)}$  are *adopted* from solution of Equations (3.18).

Two values of backlash have to be determined:  $s_{ps}^i$  between the tooth flanks of the planet and the sun gears, and  $s_{pr}^i$  between the tooth flanks of planet and ring gears.

Determination of  $s_{ps}^i$  is performed by the solution of the following systems of seven equations in seven unknowns

$$\begin{aligned}
\mathbf{r}^{(2,i)}(u_s^{(2,i)}, \dots, i_{ps}^i + 1) - \mathbf{r}^{(1)}(u_i^{(3)}, \dots, i_s^i + 1) &= \mathbf{n}^{(1)} s_{ps} \\
\left( \frac{\partial \mathbf{r}^{(1)}}{\partial u_i^{(1)}} \times \frac{\partial \mathbf{r}^{(1)}}{\partial \theta_i^{(1)}} \right) \cdot \frac{\partial \mathbf{r}^{(2,i)}}{\partial u_s^{(2,i)}} &= 0 \\
\left( \frac{\partial \mathbf{r}^{(1)}}{\partial u_i^{(1)}} \times \frac{\partial \mathbf{r}^{(1)}}{\partial \theta_i^{(1)}} \right) \cdot \frac{\partial \mathbf{r}^{(2,i)}}{\partial \theta_s^{(2,i)}} &= 0 \\
f_1(u_s^{(2,i)}, \theta_s^{(2,i)}, \psi_s^{(2,i)}, \lambda_s^{(2,i)}) &= 0 \\
f_2(u_s^{(2,i)}, \theta_s^{(2,i)}, \psi_s^{(2,i)}, \lambda_s^{(2,i)}) &= 0
\end{aligned} \tag{3.19}$$

where

$$\mathbf{n}^{(1)} = \frac{\frac{\partial \mathbf{r}^{(1)}}{\partial u_i^{(1)}} \times \frac{\partial \mathbf{r}^{(1)}}{\partial \theta_i^{(1)}}}{\left| \frac{\partial \mathbf{r}^{(1)}}{\partial u_i^{(1)}} \times \frac{\partial \mathbf{r}^{(1)}}{\partial \theta_i^{(1)}} \right|} \tag{3.20}$$

is the *outward* unit normal to the sun tooth flank surface of the  $(i_s^i + 1)^{th}$  tooth.

Determination of  $s_{pr}^i$  may be performed similarly.

If one of the two values will be negative, the corresponding tooth surfaces are candidates for the contacting ones. Then, respective teeth indexes are incremented, and Equation (3.18) is to be solved again.

### 3.3.3 Procedure for Solution

**Case 1: Planetary Gear Train with One Subtrain.** The algorithm that is represented by system of Equation (3.18) is applicable for solution of case I directly. Value of  $\phi^{(c,i)}$ ,  $i = 1$ , represents directly the angular position of the carrier  $\phi^{(c)}$ . The system of 14 equations in 14 unknowns may be solved by application of Newton-Raphson method. The result will include the position of the carrier  $\phi^{(c)}(\phi^{(1)})$ .

**Cases 2 and 3: Planetary Gear Trains With Multiple Subtrains.** Gear trains with three and five planet gears are considered, respectively. Comparing the number of equations and the unknowns, it is obtained that case 2 includes 42 unknowns, while case 3 includes 70 unknowns, to be solved simultaneously.

Attempts of direct solution of such systems did not lead to success; complexity of the transcendental equations and large number of unknowns lead to intrinsic instability of the Newton-Raphson method.

**Simplification of the Problem.** A method directed for simplification the solution of this particular system of equations is proposed. The method is based on consideration of a small number of *additional* fictitious unknowns that allow to break down the full system of equations in several systems of smaller dimension, easier to solve. Solution of the smaller systems is repeated iteratively until certain requirements on the values of the fictitious unknowns are met.

For explanation of the proposed method, we will refer to the Case 2, Figure 3.3. The carrier includes three planet gears, and angular position of the carrier is described by a unique value  $\phi^{(c)}$ .

- (1) We temporarily assume that, instead of a unique monolithic carrier, there are three carriers, one for every subtrain. The angular positions of the carriers are identified by  $\phi^{(c,i)}$ ,  $i = 1, \dots, 3$ .
- (2) The initial (guess) values of  $\Delta E_{1x}$  and  $\Delta E_{1y}$  (representing position of the axis of the sun) are considered as given.
- (3) Equation (3.18) is applied to each subtrain. Method of Newton-Raphson is applied for solution. Angles  $\phi^{(c,i)}$ ,  $i = 1, \dots, 3$ , that are obtained by the proposed approach, may differ one from each other. Note that value of  $\phi^{(c,i)}$  depends on the chosen location of the center of the sun gear

$$\phi^{(c,i)} = \phi^{(c,i)}(\Delta E_{1x}, \Delta E_{1y}) \quad (3.21)$$

- (4) The conditions of rigid, unique carrier are now applied. These conditions state that the angular position of the carrier of each subtrain has to be the same. The conditions may be represented as follows:

$$\begin{aligned} \phi^{(c,1)} - \phi^{(c,2)} &= 0 \\ \phi^{(c,2)} - \phi^{(c,3)} &= 0 \end{aligned} \quad (3.22)$$

Notice that the remaining condition,  $\phi^{(c,3)} - \phi^{(c,1)} = 0$  is automatically satisfied by Equation (3.22).

Considering that Equations (3.22) are based on unknowns  $\Delta E_{1x}$  and  $\Delta E_{1y}$ , system (3.22) may be solved for determination of the center position of the sun.

From the numerical point of view, this procedure requires application of Newton-Raphson (NR) method twice. In the first case, NR method is used to solve system (3.22). Solution of (3.22) is performed iteratively, by changing the values of  $\Delta E_{1x}$  and  $\Delta E_{1y}$  for convergence of Equation (3.22). Each time  $\Delta E_{1x}$  and  $\Delta E_{1y}$  are changed by the first case of application of NR, functions (3.21) have to be recomputed again by application of NR method for the solution of (3.18), (second case).

After the solution of Equations (3.22) is obtained, the position of the carrier is determined as  $\phi^{(c)} = \phi^{(c,1)} = \phi^{(c,2)} = \phi^{(c,3)}$ .

This method has proven to be very reliable for the case of three planet gears.

Solution of (3.22) permits the position of the center of the sun gear to be determined, as well as the errors of transmission of the carrier, defined as

$$\Delta\phi^{(c)}(\phi_1) = \phi_c - m_{c1}\phi_1 = 0 \quad (3.23)$$

where  $m_{c1}$  is the transmission ratio of the planetary gear.

### 3.4 Numerical Example

A planetary gear train corresponding to Case 2 of design is considered, see Figure 3.3. The gear data that defines the train is represented in Table 3.1.

A special computer program has been developed for the simulation of the conditions of meshing of such planetary trains. The program is based on the ideas presented above. Although only spur gears are applied in this example, the program is capable of analysis of gear drives formed by helical gears as well. The computer program has been developed for application in Windows operative system, and graphic user interface is provided for simplified input of the relevant gear data, see Figure 3.4.

Five cases are considered in the performed analysis:

- (1) Ideal gear train, without error of manufacturing and assembly
- (2) Error of indexing of the carrier  $\Delta E_t$
- (3) Error of center position of the carrier
- (4) Error of run-out (eccentricity) of the sun gear
- (5) Error of run-out of a planetary gear

For each case, two results of simulation are provided: (1) wherein the planet gears are involute gears, and (1) double crowned gears.

#### 3.4.1 Case 1: Ideal Gear Train

Considerations of this simple case are directed to test the correctness of the computer program developed.

**Involute gears.** Results of analysis for involute gears are represented in Figure 3.5(a) and (b). Results are commented as follows:

(1) Figure 3.5(a) shows the displacement of the center position of the sun gear for a revolution of the carrier. The center of the sun gears, even if it is not constrained, maintains a fixed position coinciding with the center of the mechanism.

(2) Figure 3.5(b) shows the transmission errors of the carrier, defined by application of (3.23). The abscissa represents a full revolution of the carrier. The actual position of the carrier coincides at every instant with the theoretical position, therefore there are no transmission errors.

The obtained results confirm the validity of the computer program.

**Double Crowned Gears.** If double crowning of the planet gears is applied, the situation is slightly modified as follows (Fig. 3.6(a) and (b)):

The center of the sun gear is not fixed, but performs a complicated planetary motion of very small amplitude (about 1  $\mu\text{m}$ ) (Fig. 3.6(a)).

The carrier *lags* with respect to its theoretical position of about 2 arcsec. Since this value is practically constant, it does not cause the fluctuation of velocity of driven shafts, and is not the source of torsional vibrations and noise.

**Comments.** It has to be noticed that the ability of the sun gear with free motion compensates for the existence of fluctuating transmission errors of low-amplitude. Such errors are caused by the modification of tooth geometry (of double crowning). An ordinary gear drive formed by the sun and the planet gears as designed in this example would have a parabolic function of transmission errors of 8 arcsec of amplitude.

### 3.4.2 Case 2: Error of Indexing of the Carrier

Error of indexing of the carrier is of main concern of investigation while considering the load distribution.

**Involute Gears.** Results of performed investigation are represented in Fig. 3.7(a) and (b) for the case of involute gears.

Results are interpreted as follows:

(1) Figure 3.7(a) shows the trajectory of the sun for a full revolution of the carrier. The trajectory is an exact circle. The sun gear performs therefore a planetary motion formed by: (a) rotation about its axis with angular velocity of the sun gears, and (b) rotation about the mechanism axis with the carrier angular velocity. The position of the sun gear appear fixed if it is considered in the carrier reference system.

(2) The carrier *lags* with respect to its theoretical position of about 6.4 arcsec, constant. As explained before, this errors of transmission are not the source of noise and torsional vibrations.

**Double Crowned Gears.** For the case wherein double crowning is applied, the motion of the center of the sun gear is a superimposition of results obtained in cases (1) and (2) (see Fig. 3.8):

(1) The trajectory of the sun is in an “averaged” circle, but with some superimposed small vibrations of triangular shape (see Fig. 3.8(a)).

(2) The carrier *lags* with respect to its theoretical position of about 8.2 arcsec, almost constant. These errors of transmission are not the source of noise and torsional vibrations.

**Comment 1.** Simultaneously tangency of three subtrains has been achieved for all angular positions. This is the precondition for uniform load distribution.

**Comment 2.** Notice that also in this case the errors of transmissions due to modification of gear surfaces are absorbed automatically by proper displacements of the sun gear.

**Geometrical Interpretation.** The geometrical interpretation of the effect of an error of indexing of the carrier represents a good illustration for understanding of kinematics of an isostatic planetary gear train (see Fig. 3.9).

(1) Initially, it is considered that the center of the sun gear coincides with the axis of the mechanism. Axes  $p_i - p_i$ ,  $i = 1, 2, 3$  represent the lines of action of the contacts between the sun and planet gears. The triangle that is formed by these lines is circumscribed by the base circle of the sun gear. Assuming that error  $\Delta E_i$  is small, we may consider the triangle as equilateral. Error  $\Delta E_i^{(1)}$  causes a small backlash between sun gear 1 and planet  $2^1$ . The amount of backlash, measured across line  $p_i - p_i$ , is approximately  $s = 2\Delta E_i \cos \alpha$ , where  $\alpha = 20^\circ$  is the pressure angle of the gears. Assuming  $\Delta E_i = 20 \mu\text{m}$ , we obtain  $s = 37.6 \mu\text{m}$ .

(2) This backlash has to be compensated by relative motion of the sun gear and the mechanism. Since the sun is in tangency with planet gears  $2^2$  and  $2^3$ , the motion allowed will be a *small rotation* centered at point  $O_{23}$ , defined by intersection of pressure lines  $p_2 - p_2$  and  $p_3 - p_3$ .

The angle of rotation of the sun gear is  $\Delta\phi_1 = s / \overline{O_{23}H}$ , or  $\Delta\phi_1 = s / (3r_{b1})$ , where  $r_{b1}$  is the base circle of the sun gear, and  $\overline{O_{23}H} = 3r_{b1}$ . Substituting the numbers, we obtain  $\Delta\phi_1 = 0.103 \mu\text{rad} = 21.2 \text{ arcsec}$ .

The resulting angular error, measured on the carrier, will be  $\Delta\phi_c = \Delta\phi_1 m_{c1} = 21.2 \cdot 0.301 = 6.38$  arcsec.

This value corresponds to the *increase* of lag of the carrier from the condition of an ideal train (case 1), to the condition wherein error of indexing is applied. This values perfectly agrees with the results obtained from the numerical simulation, for both cases of involute and double crowned gears.

(3) The magnitude of displacement of the center of the sun gear will be  $\Delta E_1 = \Delta\phi_1 \cdot \overline{O_{23}O_1}$ . Since  $\overline{O_{23}O_1} = 2r_{b1}$ , after substitution we obtain  $\Delta E_1 = 2s/3$ .

Substituting the numbers, we obtain  $\Delta E_1 = 25 \mu\text{m}$ , that corresponds to the radius of circle of Figure 3.7, thereby confirming the results.

### 3.4.3 Case 3: Error of Center Position of the Carrier

This example shows that errors of center position of the carrier are of no concern for this planetary gear drive. The error is absorbed by automatic relocation of the center of the sun gear.

In the case wherein involute gears are applied (Fig. 3.10(a)), the center of the sun gear is fixed in a position near the center of mechanism.

In the case of double-crowned gears (Fig. 3.11(a)), the sun gear has a vibration motion (of very small amplitude) about the position assumed by involute gears. As in previous cases, this motion allows to absorb the fluctuations of transmission errors, as shown in Figure 3.11(b).

Therefore, in both cases mentioned above the error of center position of the carrier does not cause to transmission errors that are source of torsional vibrations of the driven shaft.

### 3.4.4 Case 4: Run-Out Error of the Sun Gear

Performed analysis shows that a run-out error of the sun gear is compensated by the gear drive.

For the case of involute gears, the center of the sun will follow a circular trajectory (Fig. 3.12(a)). This circle is repeated for each revolution of the sun gear, and the circle radius corresponds to the eccentricity error. Therefore, the self-performed regulation is able to cancel the effect of the eccentricity, providing an “error” which is equal and opposite.

Also in this case, there are no errors of transmission (Fig. 3.12(b)).

A similar picture is obtained for the case of double-crowned gears, wherein additional vibration of the sun gear compensates for the effect of crowning of gear profile, similarly to Figure 3.6.

### 3.4.5 Case 5: Run-Out Error of a Planet Gear

The run-out error of the planet gear  $2^{(i)}$ ,  $i = 1$ , represents an interesting case.

The motion of the planet gear *relative to* the carrier is considered. This motion is a rotation, and the angular velocity is  $(\omega_p)_{rel} = (\omega_1 - \omega_c)N_1 / N_2 = 1.057\omega_1$ . This means that the effect of this error will have a period of  $1/1.057 = 0.9463$  revolutions of the sun gear.

Figure 3.13(a) shows the center position of the sun gear for rotation of the sun gear of 0.9463 of a revolution. The picture resemble to two petals of a trefoil. Transmission errors are not constant (Fig. 3.13(b)), but are a periodic (harmonic) shape. The period is one revolution of the planet, with respect to the carrier, that is equivalent to the 0.9463 of revolutions of the sun gear.

Figure 3.14(a) and (b) show the center position of the sun gear and transmission errors for three full revolutions of the planet, and Fig. 3.15 represents the results of 30 revolutions of the planet.

Results obtained for the double-crowned gears are similar.

### 3.5 Conclusions

In this report, conditions for design of one-stage isostatic planetary gear trains have been determined. One of the proposed designs, with three planet gears, has been the subject of numerical simulation of meshing. The simulation was directed to:

- (1) Validate the idea that such a mechanism can have simultaneous meshing even in presence of errors of alignment.
- (2) Investigate the effect of some errors of manufacturing and assembly.

An example simulation of a 3 planet system has confirmed that only the errors of run-out of the planets are the actually source of transmission errors.

It was also found that small radial vibrations of the sun gear, in the plane of the mechanism, may compensate for the transmission errors that are produced by application of mismatched tooth-profiles, as in the case of double-crowned planet gears.

In order to perform this complex numerical simulation, an original method of solution by TCA has been proposed. Algorithms for the simulation have been presented and developed. Geometrical interpretation of relevant behavior of the mechanism has been provided.

### References

1. F.L. Litvin, D. Vecchiato, A. Demenego, E. Karedes, B. Hansen, and R.F. Handschuh, *Design of One Stage Planetary Gear Train with Improved Conditions of Load Distribution and Reduced Transmission Errors*. Journal of Mechanical Design, Vol. 124, pp. 745–752, 2002.
2. F.L. Litvin, and A. Fuentes, *Gear Geometry and Applied Theory, Second Edition*. Cambridge University Press, New York, 2004.
3. F.L. Litvin, et al., *Helical and spur gear drive with double crowned pinion tooth surfaces and conjugated gear tooth surfaces*, US Patent No. 6,205,879, 2001.
4. F.L. Litvin, A. Fuentes, I. Gonzalez-Perez, L. Carnevali, K. Kawasaki, and R.F. Handschuh, *Modified Involute Helical Gears: Computerized Design, Simulation of Meshing and Stress Analysis*. Computer Methods in Applied Mechanics and Engineering, Vol. 192, pp. 3619–3655, 2003.
5. J.J. More, B.S. Garbow, and K.E. Hilstrom. *User Guide for MINPACK-1*. Argonne National Laboratory, Report ANL–80–74, Argonne, Illinois, 1980.

TABLE 3.1.—GEAR DATA FOR THE NUMERICAL EXAMPLE

| Design parameter  | Sun | Planet                | Ring |
|---|-----|-----------------------|------|
| Number of teeth, $z$                                    | 65  | 43                    | 151  |
| Module, $m$ (mm)  |     | 4                     |      |
| Pressure angle, $\alpha$ (deg)                          |     | 20°                   |      |
| Face width, $b$ (mm)                                    |     | 40                    |      |
| Addendum of the tool, $h_{a0}$ (mm)                     |     | 1.25 $m$              |      |
| Addendum of the gear, $h_a$ (mm)                        |     | $m$                   |      |
| Profile shift coefficient, $x$                          |     | 0                     |      |
| Tool parabola coefficient, $a_p$ (mm <sup>-1</sup> )    | 0   | 1.25·10 <sup>-3</sup> | 0    |
| Longitudinal parabola coeff., $a_l$ (mm <sup>-1</sup> ) | 0   | 62.5·10 <sup>-3</sup> | 0    |

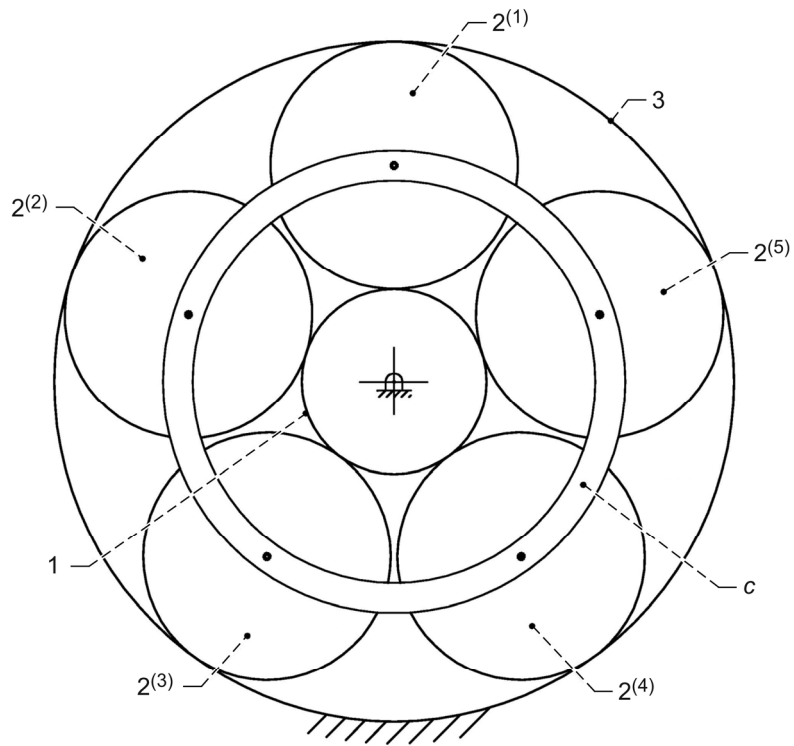


Figure 3.1.—Schematic of a planetary gear train.

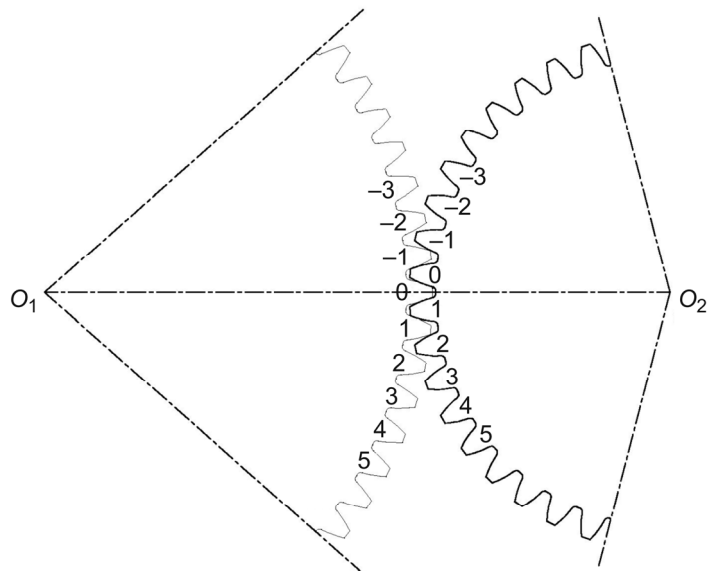


Figure 3.2.—Illustration of tooth numbering.

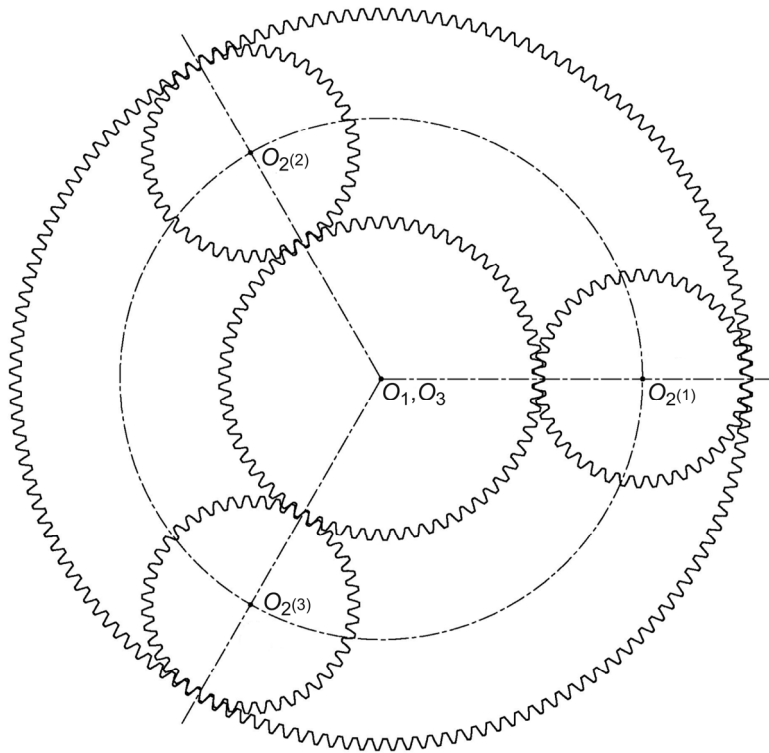


Figure 3.3.—Schematic of planetary gear train with 3 planets.

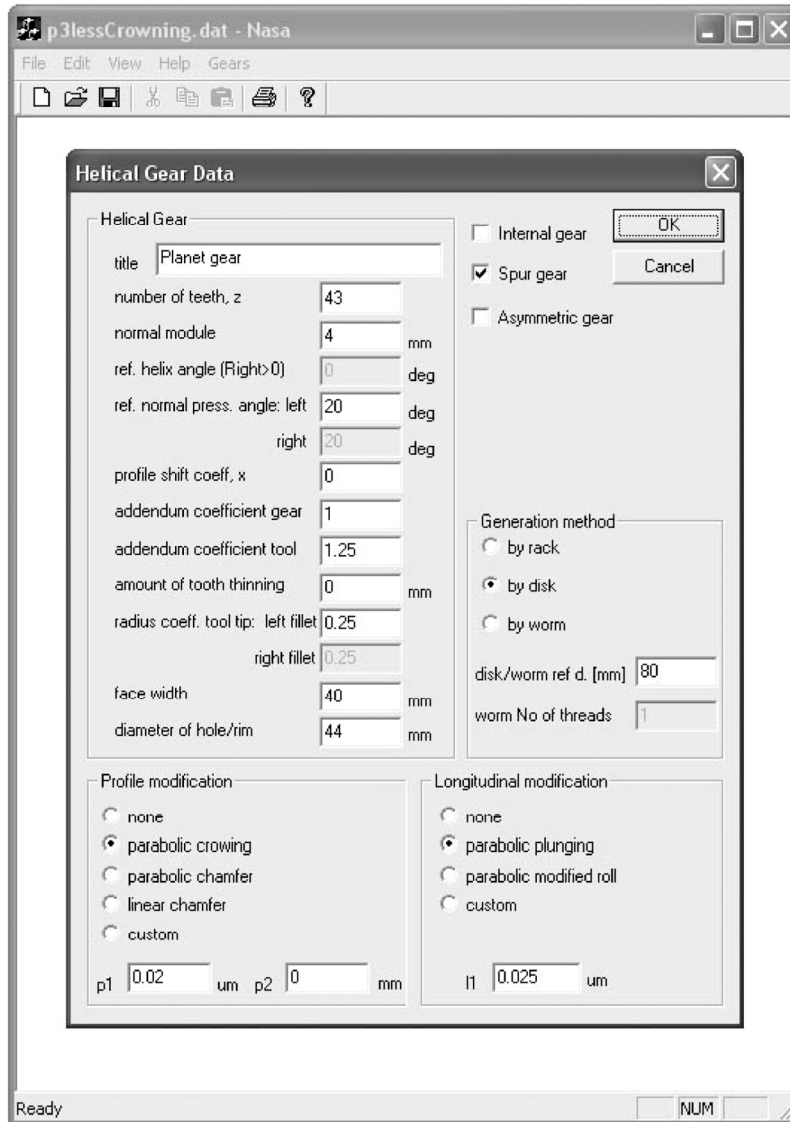


Figure 3.4.—Screen shot of user interface for developed computer program.

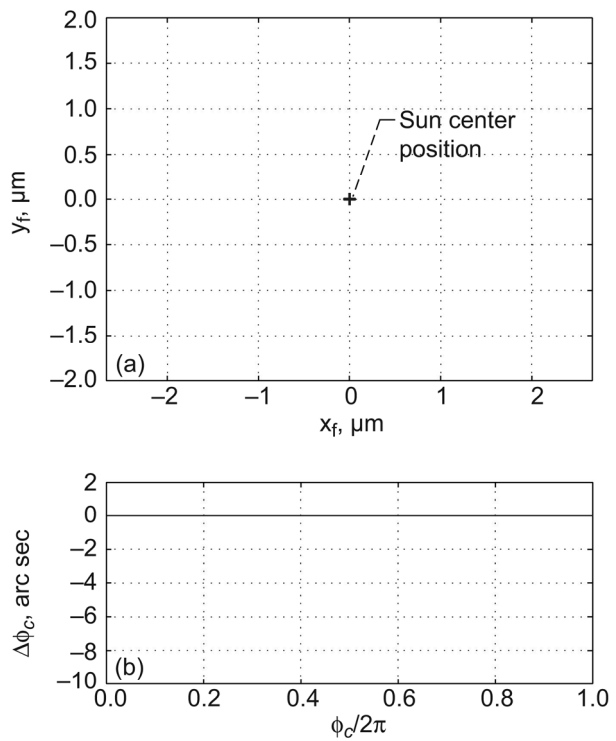


Figure 3.5.—Illustration of results obtained for involute planet gears. (a) Trajectory of sun gear. (b) Transmission errors for one revolution of the carrier.

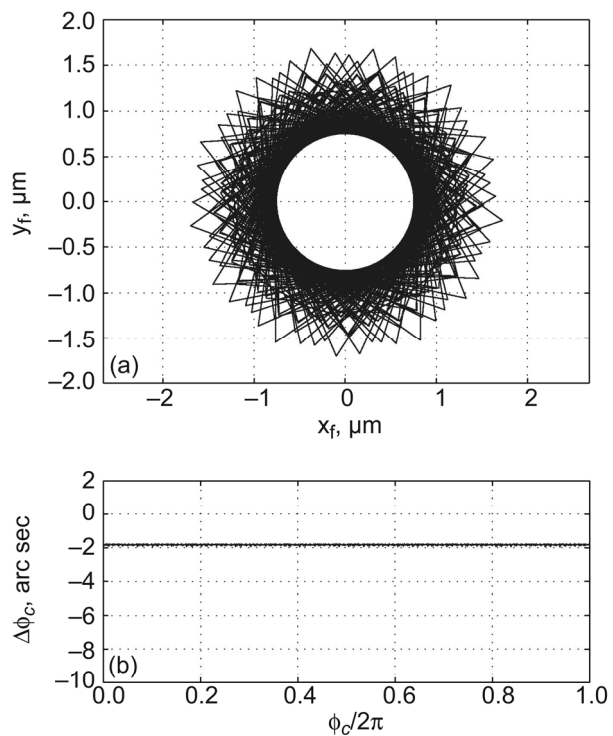


Figure 3.6.—Illustration of results obtained for double-crowned planet gears. (a) Trajectory of sun gear. (b) Transmission errors for one revolution of the carrier.

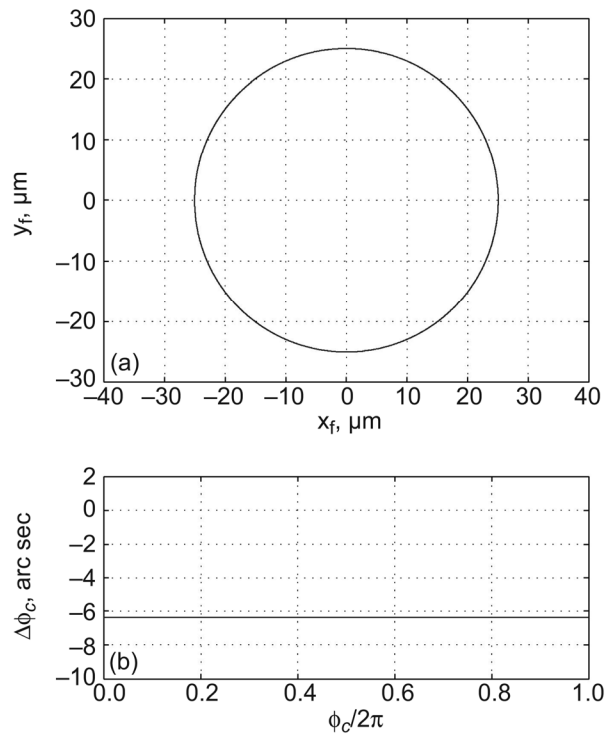


Figure 3.7.—Illustration of effect of error of indexing of the carrier  $\Delta E_p^{(1)} = 20 \mu\text{m}$ . (a) Trajectory of sun gear. (b) Transmission errors. The results correspond to application of involute planet gears and to one revolution of the carrier.

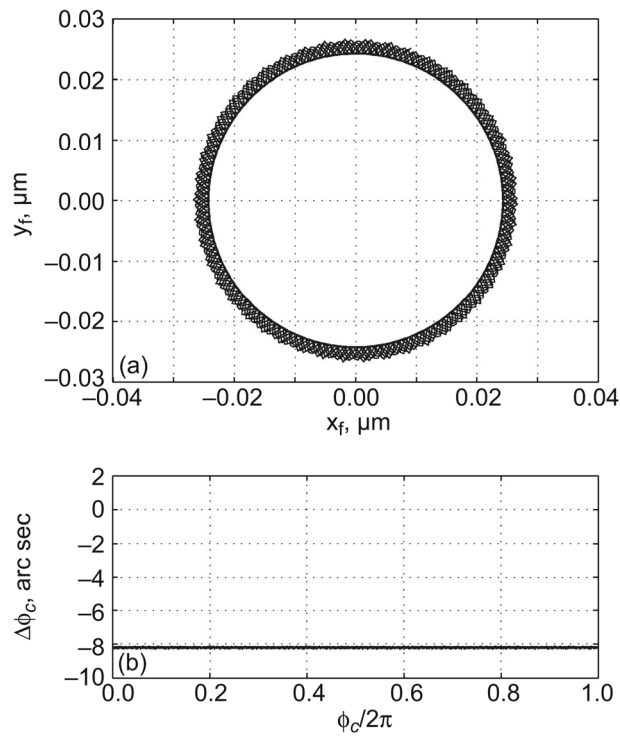


Figure 3.8.—Illustration of effect of error of indexing of the carrier  $\Delta E_f^{(1)} = 20 \mu\text{m}$ . (a) Trajectory of sun gear. (b) Transmission errors. The results correspond to application of double-crowned planet gears and to one revolution of the carrier.

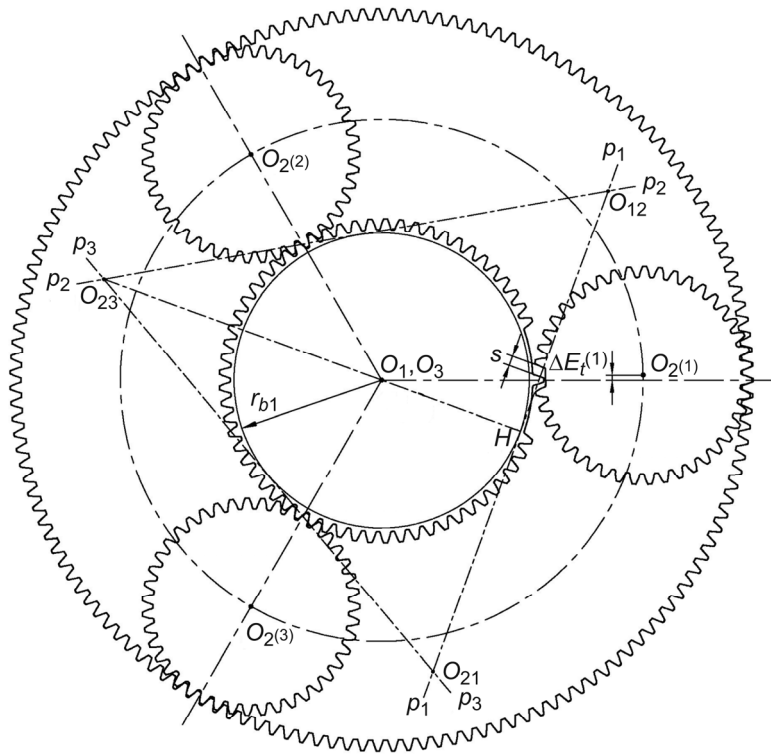


Figure 3.9.—Kinematic interpretation of effect of error of indexing of the carrier.

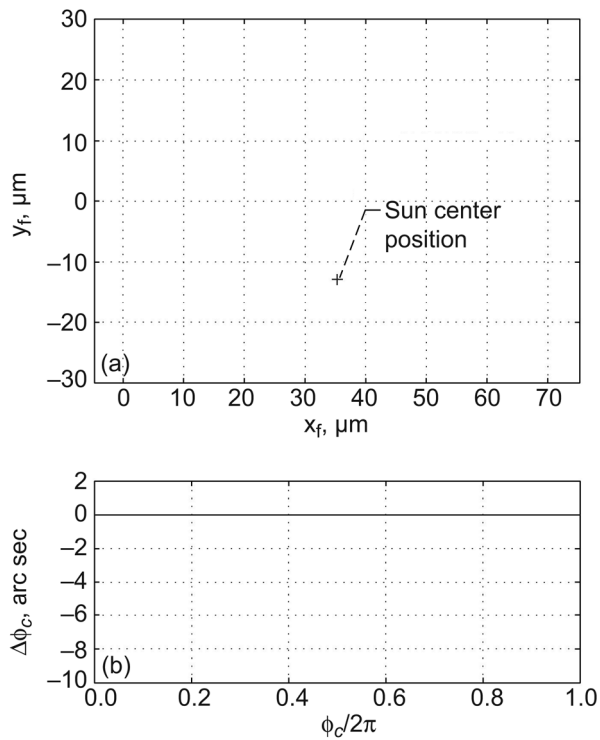


Figure 3.10.—Illustration of effect of error of the center of the carrier  $\Delta E_{cx} = 20 \mu\text{m}$ . (a) Trajectory of sun gear. (b) Transmission errors. The results correspond to application of involute planet gears and to one revolution of the carrier.

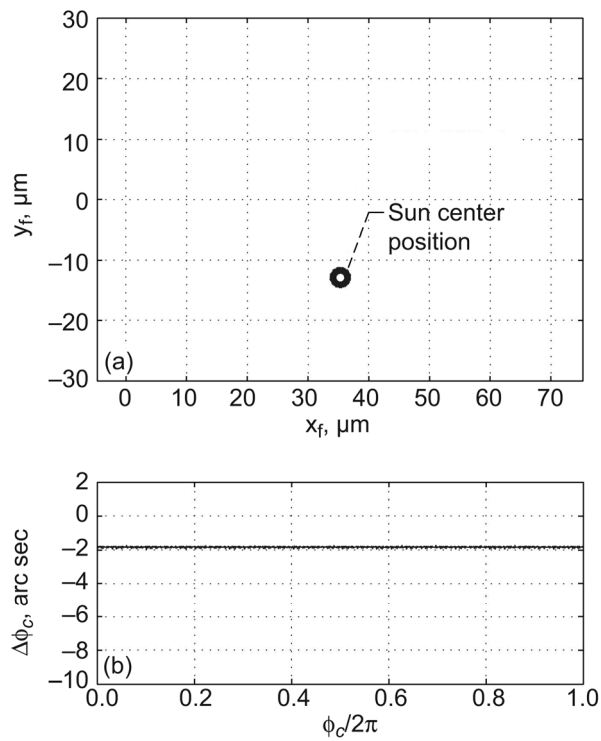


Figure 3.11.—Illustration of effect of error of the center of the carrier  $\Delta E_{cx} = 20 \mu\text{m}$ . (a) Trajectory of sun gear. (b) Transmission errors. The results correspond to application of double-crowned planet gears and to one revolution of the carrier.

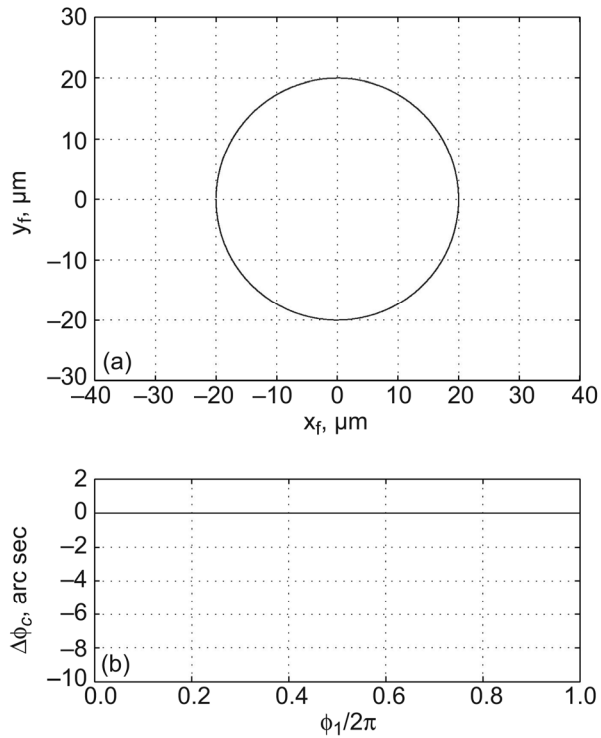


Figure 3.12.—Illustration of effect of error of run-out of the sun gear  $\epsilon_r^{(1)} = 20 \mu\text{m}$ . (a) Trajectory of sun gear. (b) Transmission errors. The results correspond to application of involute planet gears and to one revolution of the sun gear.

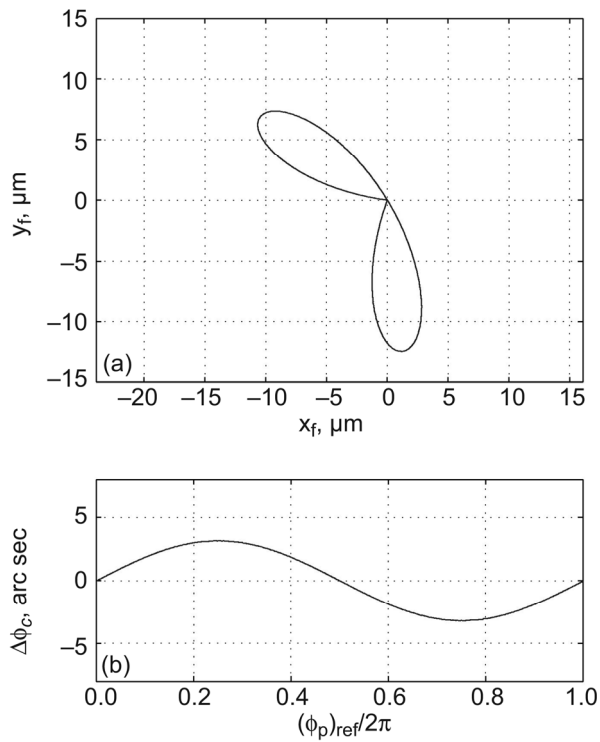


Figure 3.13.—Illustration of effect of error of run-out of the planet gear  $\varepsilon_p^{(1)} = 20 \mu\text{m}$ . (a) Trajectory of sun gear. (b) Transmission errors. The results correspond to application of involute planet gears and to one revolution of the planet gear  $2^{(1)}$ .

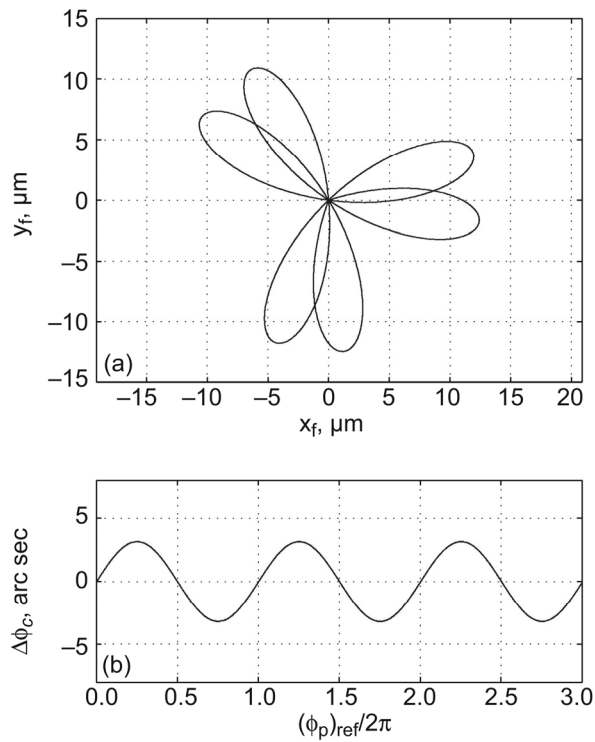


Figure 3.14.—Illustration of effect of error of run-out of the planet gear  $\varepsilon_p^{(1)} = 20 \mu\text{m}$ . (a) Trajectory of sun gear. (b) Transmission errors. The results correspond to application of involute planet gears and to three revolutions of the planet gear  $2^{(1)}$ .

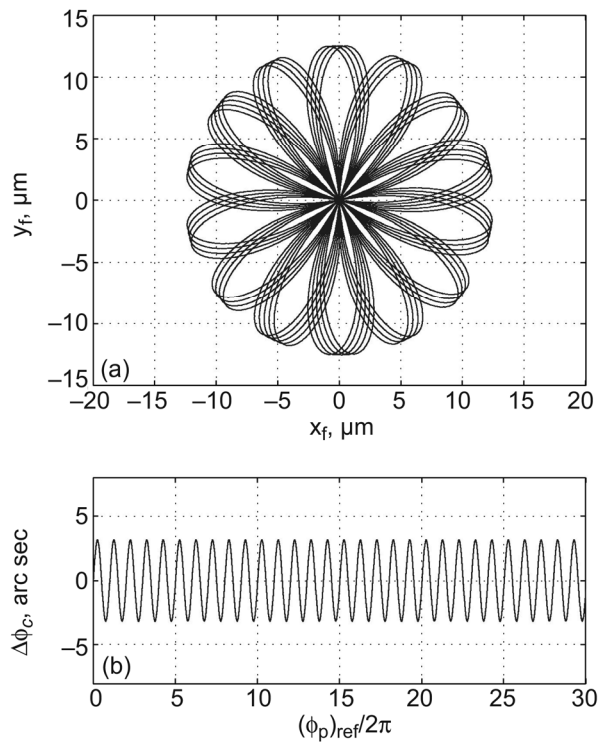


Figure 3.15.—Illustration of effect of error of run-out of the planet gear  $\varepsilon_p^{(1)} = 20 \mu\text{m}$ . (a) Trajectory of sun gear. (b) Transmission errors. The results correspond to application of involute planet gears and to thirty revolutions of the planet gear  $2^{(1)}$ .

| <b>REPORT DOCUMENTATION PAGE</b>   |   |  | <i>Form Approved</i><br><i>OMB No. 0704-0188</i>  |  |
|--|---|--|---|--|
| Public reporting burden for this collection of information is estimated to average 1 hour per response, including the time for reviewing instructions, searching existing data sources, gathering and maintaining the data needed, and completing and reviewing the collection of information. Send comments regarding this burden estimate or any other aspect of this collection of information, including suggestions for reducing this burden, to Washington Headquarters Services, Directorate for Information Operations and Reports, 1215 Jefferson Davis Highway, Suite 1204, Arlington, VA 22202-4302, and to the Office of Management and Budget, Paperwork Reduction Project (0704-0188), Washington, DC 20503. |   |  |   |  |
| <b>1. AGENCY USE ONLY (Leave blank)</b>  |   | <b>2. REPORT DATE</b><br>December 2005                         | <b>3. REPORT TYPE AND DATES COVERED</b><br>Final Contractor Report                              |  |
| <b>4. TITLE AND SUBTITLE</b><br><br>Design of Gear Drives With High Gear Ratio   |   |  | <b>5. FUNDING NUMBERS</b><br><br>WBS-22-714-90-03<br>NAG3-2450<br>1L162211A47A                  |  |
| <b>6. AUTHOR(S)</b><br><br>Faydor L. Litvin, Alfonso Fuentes, Daniele Vecchiato,<br>and Ignacio Gonzalez-Perez   |   |  |   |  |
| <b>7. PERFORMING ORGANIZATION NAME(S) AND ADDRESS(ES)</b><br><br>University of Illinois at Chicago<br>601 S. Morgan Street<br>Chicago, Illinois 60607  |   |  | <b>8. PERFORMING ORGANIZATION REPORT NUMBER</b><br><br>E-15325                                  |  |
| <b>9. SPONSORING/MONITORING AGENCY NAME(S) AND ADDRESS(ES)</b><br><br>National Aeronautics and Space Administration<br>Washington, DC 20546-0001<br>and<br>U.S. Army Research Laboratory<br>Adelphi, Maryland 20783-1145   |   |  | <b>10. SPONSORING/MONITORING AGENCY REPORT NUMBER</b><br><br>NASA CR-2005-214002<br>ARL-CR-0569 |  |
| <b>11. SUPPLEMENTARY NOTES</b><br><br>Project Manager, Robert F. Handschuh, Structures Division, U.S. Army Research Laboratory, Vehicle Technology Directorate, NASA Glenn Research Center, organization code RSM, 216-433-3969.   |   |  |   |  |
| <b>12a. DISTRIBUTION/AVAILABILITY STATEMENT</b><br><br>Unclassified - Unlimited<br>Subject Category: 37<br><br>Available electronically at <a href="http://gltrs.grc.nasa.gov">http://gltrs.grc.nasa.gov</a><br>This publication is available from the NASA Center for AeroSpace Information, 301-621-0390.  |   |  | <b>12b. DISTRIBUTION CODE</b>   |  |
| <b>13. ABSTRACT (Maximum 200 words)</b><br><br>A three part paper to describe the results of several gear drive types with a high gear ratio is presented. A single stage planetary gear train with double helical gears is described with methods to reduce transmission errors and improve load distribution by regulating backlash during assembly. A new arrangement for face gear is also described. This new mechanism can perform rotations between axes that are collinear and intersected. Finally the design and simulation of an isostatic planetary gear train is presented. Conditions that can lead to noise and vibration of the planetary gear drive are described.  |   |  |   |  |
| <b>14. SUBJECT TERMS</b><br><br>Gears; Transmissions   |   |  | <b>15. NUMBER OF PAGES</b><br>66  |  |
|  |   |  | <b>16. PRICE CODE</b>   |  |
| <b>17. SECURITY CLASSIFICATION OF REPORT</b><br>Unclassified   | <b>18. SECURITY CLASSIFICATION OF THIS PAGE</b><br>Unclassified | <b>19. SECURITY CLASSIFICATION OF ABSTRACT</b><br>Unclassified | <b>20. LIMITATION OF ABSTRACT</b>   |  |



